Master's thesis

NTNU
Norwegian University of Science and Technology
Faculty of Engineering
Department of Geoscience and Petroleum

Endre Refsnes

Simulation of Pressure Pulses in Top-hole Cementing Operations

Master's thesis in Petroleum Geosciences and Engineering
Supervisor: Sigbjørn Sangesland
June 2020

NTNU
Norwegian University of
Science and Technology

Endre Refsnes

Simulation of Pressure Pulses in Top-hole Cementing Operations

Master's thesis in Petroleum Geosciences and Engineering
Supervisor: Sigbjørn Sangesland
June 2020

Norwegian University of Science and Technology
Faculty of Engineering
Department of Geoscience and Petroleum

NTNU
Norwegian University of
Science and Technology

Preface

This thesis was carried out by the undersigned candidate as a final assignment in the pursue of a Master of Science in Petroleum Engineering, with specialization within drilling technology. The thesis was written during the spring semester of 2020 at the Department of Petroleum Engineering and Applied Geophysics at the Norwegian University of Science and Technology.

This thesis investigates the phenomenon of pressure pulses from launching the wiper plugs in top-hole cementing operations. Development and magnitude of these pressure pulses are explored through simulations in a digital model, constructed in Matlab.

Trondheim, 10/6/2020

Endre Refsnes

Endre Refsnes

Acknowledgements

I want to thank my supervisor Professor Sigbjørn Sangesland at NTNU for the opportunity to work on an exciting and challenging topic for my thesis. His advices and guidance have been very useful for developing a good approach to the topic, but also helpful in the process of writing this thesis.

A great thanks to my co-supervisor, associated professor Behzad Elahifar, for providing me with information and advices through the work process. His enthusiasm and will for sharing operational experience have provided me an increased understanding for how top-hole drilling and cementing operations are performed. This information has been highly useful for writing my thesis.

I also want to give a special thanks to Lars Johan Sandvik for providing me with a remote desktop solution during the Covid-19 situation. The solution gave me access to powerful computing capacity from outside of the closed campus area, which was crucial for performing the simulation part of this thesis.

Last but not least, a great gratitude to my fellow students at NTNU for contributing to five magnificent years as students in Trondheim. Finally, a special remark goes to Bård Sandahl and Christoffer Sørgård for a great exchange semester at Texas A&M University.

Summary

This thesis investigates the development of pressure pulses from launching the wiper plugs in top-hole cementing operations. In this context, top-hole refers to the uppermost sections of a well, which is drilled without the blow out preventer and marine drilling riser installed. The objective has been to explore the phenomenon and evaluate the magnitude of downhole pressure. In addition, focus has been directed towards design characteristics of the top-hole system and how these parameters affect the energy loss of the propagating pressure pulse. The phenomenon, which is not much discussed in literature, can potentially cause damage to the formation and to subsea installed drilling equipment. Therefore, increased knowledge on the topic is of great interest.

The approach for exploring the phenomenon has been to construct a digital model of the top-hole system, and then perform simulations of pressure development for several different cases. A study on fundamental characteristic of top-hole drilling and cementing operations has been conducted to provide a solid fundament for the digital model. This theoretical fundament is provided in two separate chapters. The first one describes basic methods and challenges found in top-hole drilling and cementing operations, but also basic theory on pressure waves and the pressure pulse phenomenon. The second one describes the setup and applications of a riserless mud recovery system, which was implemented in the digital model.

The digital model was built in Matlab R2020a by use of the Simscape Fluid tool package, with the intention of accessing valuable knowledge on the pressure pulse phenomenon. A detailed description of the model is provided, with explanations of key components, assumption, fundamental equations and non-Newtonian rheology models.

The simulations provided values for the downhole pressure and for the energy losses across system components. Simulated results state that the bottom hole formation will be exposed to an additional pressure of 10,21 - 18,54 bar from the pulse, depending on the system design. In addition, results indicate that 65,2 – 82,0% of the total energy loss is taken across the float valves in the shoe track.

It is recommended that further work is invested to increase the level of confidence for the simulated results. The main focus in this work should be directed towards improvement of fluid system boundary conditions and float valve representation. Recommended solutions for this purpose are evaluation of alternative simulation software's and search for improved knowledge through experimental activities or through information from the industry.

Sammendrag

Denne masteroppgaven undersøker utviklingen av trykkpulser i topphullseksjoner, frembrakt fra utstøting av sementplugger under sementeringsoperasjoner. Topphull refererer i denne sammenheng til de øverste seksjonene av en brønn, som blir boret uten utblåsningssikring og marint stigerør. Målet med oppgaven har vært å utforske trykkpulsfenomenet og evaluere størrelsen av trykket i borehullet. I tillegg har fokus blitt rettet mot design faktorer ved topphullsystemet og hvordan disse påvirker energitapet til den forplantende trykkpulsen. Fenomenet, som ikke er mye omtalt i litteraturen, kan potensielt forårsake skade på formasjon og på havbunnsinstallert boreutstyr. Økt kunnskap på dette feltet er derfor av stor interesse.

Tilnærmingen for å utforske fenomenet har vært å konstruere en digital modell av topphullsystemet, og deretter utføre simuleringer av trykkutvikling for flere ulike tilfeller. En grunnleggende studie av bore- og sementeringsoperasjoner i topphullseksjoner, har blitt utført for å skape et solid fundament for den digitale modellen. Dette teoretiske fundamentet blir presentert i to ulike kapitler. Det første beskriver grunnleggende metoder og utfordringer ved bore- og sementeringsoperasjoner i topphullseksjoner, men også grunnleggende teori for trykkbølger og trykkpulsfenomenet. Det andre kapitlet beskriver oppsettet og applikasjonene til et stigerørsfritt system for returnering av boreslam, som ble implementert i modellen.

Den digitale modellen ble konstruert i Matlab R2020a ved bruk av verktøypakken Simscape Fluids. Hensikten med modellen var å få tilgang til verdifull kunnskap om trykkpulsfenomenet. En detaljert beskrivelse av modellen blir presentert med forklaringer av nøkkelkomponenter, antakelser, grunnleggende ligninger og ikke-newtonske reologimodeller.

De utførte simuleringene gav verdier for trykk i borehullet og for energitap forårsaket av komponenter i systemet. Ifølge de simulerte resultatene, så vil formasjonen i bunnen av borehullet bli utsatt for et ekstra trykk på 10,21 – 18,54 bar fra pulsen, avhengig av systemets design. I tillegg indikerer resultatene at 65,2 – 82,0% av det totale energitapet blir forårsaket av tilbakeslagsventilene i foringsrøret.

Videre arbeid anbefales for å øke graden av troverdighet for de simulerte resultatene. Hovedfokuset i dette arbeidet bør rettes mot forbedringer av fluidsystemets grensebetingelser og modellering av tilbakeslagsventiler. Anbefalte løsninger for dette formålet er evaluering av alternative simuleringsprogrammer og søk etter forbedret kunnskap gjennom eksperimenter eller ved informasjon fra industrien.

Table of Contents

Preface I
Acknowledgements III
Summary V
Sammendrag VI
List of Figures X
List of Tables XI
1 Introduction 1
2 Top-hole Drilling and Cementing 3
2.1 Top-hole Drilling Practice 4
2.1.1 Conductor Section 4
2.1.2 Conductor Anchor Node (CAN) Technology 7
2.1.3 Conductor Shoe Setting Depth 9
2.1.4 Surface Casing Section 12
2.2 Top-hole Cementing Practice 13
2.2.1 Objective and Requirements 13
2.2.2 Cementing Equipment and Displacement Procedure 14
2.2.3 Design of Cement Slurries and Spacer Fluids 17
2.2.4 Challenges in Top-Hole Cement Operations 17
2.3 Basic Wave Theory 18
3 Riserless Mud Recovery (RMR) System 19
3.1 System Components 19
3.1.1 Suction Module 20
3.1.2 Subsea Pump Module 21
3.1.3 Mud Return Line 22
3.1.4 Umbilical and Winch 23
3.1.5 Deck Installed Containers 23
3.1.6 Installation Procedure 24
3.2 Primary Drivers for Using Riserless Mud Recovery Systems 25
3.2.1 Improved Well Control 25
3.2.2 Increased Setting Depth of Surface Casing 26
3.2.3 Reduced Impact on the Marine Environment 27
3.2.4 Manage Pressure Cementing 27
4 Simulations 29
4.1 Background for Simulations 29

4.2 Case Description 30
4.3 Software 32
4.4 Discretization and Fundamental Equations 32
4.5 Hydraulics 36
4.5.1 Rheology and Flow Regime 36
4.5.2 Friction Loss Model Newtonian Fluids 38
4.5.3 Friction Loss Model for non-Newtonian Fluids 39
4.6 Wellbore Pressure Regime 42
4.6.1 Equivalent Circulating Density (ECD) 42
4.6.2 Transient Pressure and Signal Generator 42
4.6.3 Thermal Effects 44
4.7 Assumptions 45
4.7.1 Digital Representation of Float Valves 45
4.7.2 Hydraulics and Fluid Properties 46
4.7.3 Pressure Pulse 47
4.7.4 Well and Equipment 47
4.8 Explanation of the Program Code 49
5 Results 51
5.1 Base Case 52
5.2 Dampening Effects 57
5.2.1 Extended Setting Depth 57
5.2.2 Float Valve Diameter 60
5.2.3 Effect of the Discharge Coefficients 61
5.2.4 Casing Size 63
5.3 Enclosed System 65
6 Discussion 66
6.1 Applicability of Using Simscape Fluids as Simulation Software 66
6.2 Validity of Simulated Results 67
6.3 Effects on Formation and Equipment 69
6.4 Recommendations for Future Work 70
7 Conclusion 71
Nomenclature 72
References 74
Appendix A: Well Trajectory for Shallow Reservoir Layer 76
Appendix B: Calculation of Jetted Conductor Lengths 77

Appendix C: Acceptance Criteria for Casing Float Valves 80
Appendix D: Steps in Conventional Cementing 81
Appendix E: Illustration of the Physical Case 82
Appendix F: Overview Digital Model 83
Appendix G: Block Descriptions 84

List of Figures

Figure 1: West Vanguard shallow gas blowout 1985 (Bøe 2011) 4
Figure 2: Riserless Drilling System (Integrated Ocean Drilling Program (IODP) 2010)..... 6
Figure 3: Subsea Hammer (Van Noort et al. 2009) 6
Figure 4: CAN about to be installed in the Barents Sea in 2018 (Neodrill AS 2020) 8
Figure 5: Conductor integrated into CAN (Mathis et al. 2017) 8
Figure 6: Rigid-bar Centralizer used on casing exterior (Weatherford International 2016).... 15
Figure 7: Float collar (left) and float shoe (right) (Weatherford International 2005)..... 15
Figure 8: Wiper plugs (left) and darts (right) (Weatherford International 2013) 16
Figure 9: Setup for the riserless mud recovery system (Stave, Nordas, et al. 2014) 19
Figure 10: SMO mud level monitored by cameras and lights (Smith et al. 2010) 21
Figure 11: Suction module (Enhanced Drilling 2020)..... 21
Figure 12: Subsea pump module (Claudey et al. 2016)..... 22
Figure 13: Staged pump configuration (Claudey et al. 2016)..... 22
Figure 14: Effect of a dual gradient drilling system in terms of increased surface casing setting depth (Claudey et al. 2016) 26
Figure 15: Manage pressure cementing (MPC) system (Elahifar 2020). 28
Figure 16: Sketch of the physical case that was modelled (Made by the author, with cuts from (Weatherford International 2005), (Weatherford International 2013) and (Elahifar 2020)..... 31
Figure 17: Illustration of the Nyquist sampling theorem (The MathWorks Inc. 2020a) 33
Figure 18: Discretized pipe with port A and port B (The MathWorks Inc. 2020a)..... 33
Figure 19: Reynolds number vs. flow and pressure drop (Brechan et al. 2017)..... 37
Figure 20: Bingham plastic model (made by the author) 40
Figure 21: Pressure signal generator (cut from model) 43
Figure 22: Pressure pulse signal from signal generator (cut from model)..... 44
Figure 23: Pressure at bottom hole. Base case with sea water as drill fluid 53
Figure 24: Pressure at the conductor shoe. Base case with sea water as drill fluid 53
Figure 25: Pressure at bottom hole. Base case with WBM #1 as drill fluid 54
Figure 26: Pressure at the conductor shoe. Base case with WBM #1 as drill fluid 55
Figure 27: Pressure at bottom hole. Base case with WBM #2 as drill fluid 56
Figure 28: Pressure at the conductor shoe. Base case with WBM #2 as drill fluid 56
Figure 29: Pressure drop across the shoe track versus valve diameter 61
Figure 30: Pressure drop across shoe track vs. discharge coefficient..... 62
Figure 31: Frictional pressure loss vs. casing size 64
Figure 32: Well trajectory with shallow kick off point (Mathis et al. 2017) 76
Figure 33: Acceptance criteria for casing float valves (Standards Norway 2004) 80
Figure 34: Steps in conventional cementing of casing strings (Brechan et al. 2017)..... 81
Figure 35: Sketch of the physical case that was modelled (made by the author, with cuts from (Weatherford International 2005), (Weatherford International 2013) and (Elahifar 2020)..... 82
Figure 36: Illustration of the digital model in block scheme format (cut from model) 83

List of Tables

Table 1: Soil conditions from geological assessment (Mathis et al. 2017) 9
Table 2: CAN- dimensions and axial load capacity (Mathis et al. 2017) 10
Table 3: Comparison of conductor lengths based on installation methods 11
Table 4: Input parameters for Eq. (4.25) 43
Table 5: Fluid properties used in model 46
Table 6: Parameters for base case simulations 47
Table 7: Wellbore pressure development for sea water 52
Table 8: Wellbore pressure development for WBM #1 54
Table 9: Wellbore pressure development for WBM #2 55
Table 10: Wellbore pressure development - Setting depth 600m BML with WBM #1 58
Table 11: Wellbore pressure development - Setting depth 600m BML with WBM #2 58
Table 12: Wellbore pressure development - Setting depth 700m BML with WBM #1 59
Table 13: Wellbore pressure development - Setting depth 700m BML with WBM #2 59
Table 14: Valve diameter vs. pressure drop across shoe track 60
Table 15: Discharge coefficient vs. pressure drop across shoe track 62
Table 16: Frictional pressure loss vs. casing size 63
Table 17: Pulse magnitude at the bottom hole, conductor shoe and top annulus 64
Table 18: Wellbore pressure development for an enclosed top-hole system 65
Table 19: Input data and results for jetted conductor lengths 79

1 Introduction

The offshore oil and gas industry are continuously developing ever-more challenging prospects in order to keep up with the global energy demand. Several of these prospects contain shallow formations with narrow drilling windows, and where small margins are left for transient pressure in the wellbore. The drilling window is defined as the drillable pressure profile, which is bounded by the formation pressure at the low side and the fracture pressure at the upper side (IADC 2020). Exceeding these boundaries can cause severe problems and safety concerns for the operation. It is therefore important to investigate the mechanisms that induce transient pressure events in the wellbore and evaluate if their magnitude can conflict the boundaries of the drilling window.

This thesis will investigate a transient pressure phenomenon found in offshore cementing operations, which occur during displacement of cement down a casing string. When the dart lands in the wiper plug, pumping continues until the differential pressure across the plug exceeds the strength of the shear pins. The wiper plug is then released and the stored energy across the plug creates a wave of compressed fluid that propagates down the casing string. Depending on pressure amplitude, this pulse can potentially cause damage to the formation or to subsea installed equipment. There exist little available literature and research describing this specific phenomenon, which makes further investigation of the topic highly interesting. In addition, improved knowledge on pressure transients and actuating mechanisms are important for adequate pressure management in the wellbore. The topic therefore of great interest to the industry.

This thesis explores the transient pressure phenomenon through a digital simulation model. The model was constructed based on fundamental knowledge of wellbore systems and downhole mechanisms. The area of focus for the model is directed to the top-hole sections, with cementing of the surface casing as the main objective. Top-hole sections refer to the uppermost sections of the well, which are drilled without the blow out preventer (BOP) and marine drilling riser installed. In some cases, conventional techniques for drilling and cementing proves inapplicable for these shallow formations due to narrow drilling windows. Modern technologies like riserless mud recovery (RMR) systems are therefore utilized to manipulate the downhole pressure and to maintain it within the boundaries. The presence of this technology was implemented into the digital model, with the purpose of simulating transient effects in a manage pressure cementing (MPC) operation.

The structure of this master thesis comprises chapters on fundamental theory, description of the simulations, results and discussions. As a commencement, the fundamental theory is presented in two separate chapters. The first one describes basic wave theory and fundamentals of top-hole drilling and cementing operations, while the second one describes the architecture and applications of riserless mud recovery systems. A detailed description of the digital model and the simulations then follows. The chapter carefully explains the simulated case, assumptions and models used in the design phase. Simulated results and discussions then follow in the last parts of the thesis. In addition, the digital model and simulation files are provided as attachments on a disc at the last page.

2 Top-hole Drilling and Cementing

The top-hole sections define the area of interest for this master thesis. The following chapter will therefore provide fundamental knowledge on top-hole drilling and cementing operations. In addition, the chapter will present fundamental wave theory for mechanical waves in fluid systems. The term top-hole refers to the two uppermost sections of the well, usually with hole sizes of 36 inches and the 26 inches (Brechan et al. 2017). These sections define the well foundation, which has the purpose of providing a solid base for the well construction and production phase. An important aspect is therefore the ability to carry high loads from the large blow out preventer (BOP), marine drilling riser and subsequent casing strings. The foundation must also withstand fatigue loads and bending moments from wellhead installed equipment. In other words, the well foundation must withstand the worst case scenario of forces and loads through the entire life of the well, in order to preserve the well integrity (Prasertamporn 2016).

Today, riserless drilling is the conventional technique utilized on top-hole sections at the Norwegian Continental Shelf (NCS). The technique has emerged from operational experience and technology improvements in the early phase of Norwegian oil production. Before 1987, it was conventional procedure to drill all bit sections with the marine drilling riser installed and with a gas diverter system below the drill floor for handling any gas influxes (Skalle 2015). The major disadvantage with this system was the great safety risk of guiding massive gas volumes directly to the drilling vessel, in case of a shallow gas blowout. In 1985, this risk became particularly evident when the drilling vessel West Vanguard experienced a shallow gas blowout in the Haltenbanken area (Skalle 2015). Figure 1 shows how the gas flows up below the rig and reduces the buoyancy. One life was lost and the well blew out for five months before it was plugged (Smith-Solbakken and Vinnem 2020). The accident report concluded that changes in the drilling procedure were necessary. The conventional procedure has therefore become to drill the top-hole sections without the marine drilling riser installed (Skalle 2015).

Figure 1: West Vanguard shallow gas blowout 1985 (Bøe 2011)

2.1 Top-hole Drilling Practice

Drilling the top-hole sections from floating drilling vessels can be demanding, and several techniques have been developed over the years for managing these challenges. This section provides basic information on methods and equipment utilized in top-hole drilling and cementing operations. Some characteristic features of drilling shallow formations are also presented, with explanations for how these affect the installation method and setting depth of the casing strings.

2.1.1 Conductor Section

The first step of the well construction process is called spudding. It is carried out by creating the uppermost hole section, often referred to as the conductor section. There are several methods available for this purpose within the industry. The conventional one is to drill a 36 inch hole, then run a 30 inch conductor casing and cement it into place. The setting depth for this casing string will vary for each well location, but is typically 200-250ft below mud line (BML) (Reksterberg and Kvassheim 2011). As mentioned earlier, the operation is usually performed riserless by use of the pump and dump method, illustrated in Figure 2. This implies that all returns of drill fluid and solids are discharged to the seabed. Sea water is normally

used as drill fluid for this section, because it is easy accessible in large volumes and it complies with environmental regulations (Brechan et al. 2017). Techniques for returning drill fluid and solids back to the drilling vessel will be presented in Chapter 3 and they provide an alternative to the pump and dump method.

Conductor jetting is a second method for constructing the conductor section and it is frequently used in deepwater locations. The method is based on hydraulically washing the formation below the conductor casing throughout the installation process (Prasertamporn 2016). A jetting assembly is used for this purpose and it consists of a bit, a mud motor and a running tool. The bit is placed slightly below the casing shoe to hydraulically wash the formation as the string is lowered into the seabed. Bit rotation is provided by the mud motor through circulation of drill fluid. During the installation process, all returns are taken inside the conductor casing and discharged to the seabed. The running tool is installed in the upper part of the jetting assembly and it is constructed with a release function. This allows the assembly to be released in case of operational difficulties or when reaching the installation depth. The release function also enables drilling of the subsequent section directly after conductor installation, without making an additional trip out of the hole (Prasertamporn 2016).

A third method for conductor installation is conductor driving. This method is based on using a hydraulic hammer to drive the conductor casing into the seabed, like illustrated in Figure 3. Conductor driving has traditionally been a method used for shallower waters, where the hammer is situated on the rig floor of jack-up rigs. However, development of subsea hydraulic hammers in later years has enabled the method to be used for significant water depths as well. For instance, conductors have been installed in water depths up to 1920m at the Parque das Conchas field, situated offshore Brazil (Van Noort et al. 2009).

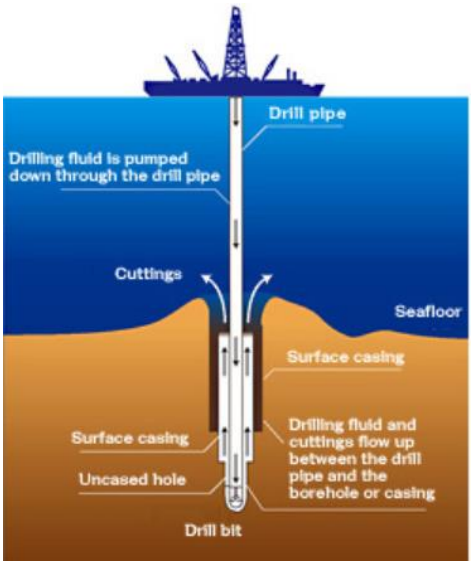

Figure 2: Riserless Drilling System (Integrated Ocean Drilling Program (IODP) 2010)

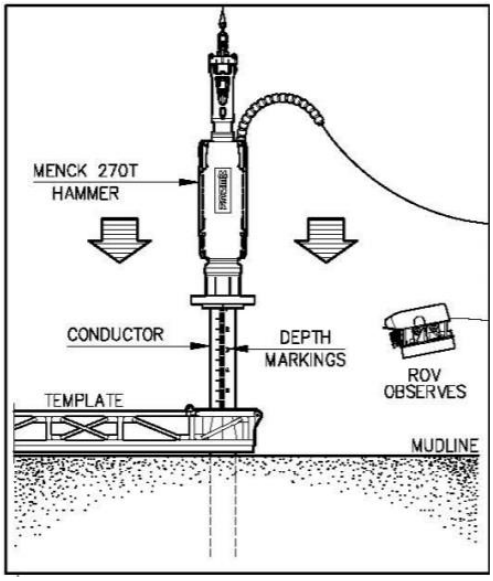

Figure 3: Subsea Hammer (Van Noort et al. 2009)

Conductor installation is usually a quick and uncomplicated procedure in shallow water depths, like most areas on the Norwegian Continental Shelf. However, this is usually not the case for deepwater and ultra-deepwater areas like in the Gulf of Mexico, where the installation process tends to be more complicated (Reksterberg and Kvassheim 2011). Some complicating factors are great water depths, strong environmental forces and unconsolidated soil conditions. For instance, environmental forces like ocean currents and waves will affect the drilling vessel during the operation. Accurate dynamic positioning (DP) systems and powerful thrusters are therefore required to maintain the vessel position over the well location. A remotely operated vehicle (ROV) is also required at permanent basis for observation and for guiding of equipment into the wellbore (Reksterberg and Kvassheim 2011).

In addition, the great water depth causes tripping operations to be highly time consuming. Combined with the high day rates for modern drilling vessels, it is beneficial to spend as little time as possible on these operations. Therefore, conductor jetting has been the preferred method in great water depths, as it allows for running the next section drilling assembly together with the conductor (Prasertamporn 2016). Drilling of the subsequent section can then commence directly after the conductor is installed and without having to trip back to the vessel. Top-hole drilling operations can also be performed in campaigns. This provides an opportunity to improve the overall time efficiency and to reduce the cost drilling vessels. The

method applies for situation where multiple top-holes are planned in the same area, for instance during a new field development.

The soil conditions of shallow formations are an important aspect for the conductor installation process. If the conductor is tilted more than 1-2° or if it starts subsiding after installation is completed, then re-spud of the borehole is a likely consequence (Brechan et al. 2017). Degree of sediment consolidation is therefore important, as more consolidation yields more support to the conductor pipe. As the sediment consolidation normally decreases with increasing water depth, the ground conditions can become a problem in deepwater environments. The low soil strength may cause difficulties in achieving a complete cement displacement around the conductor casing and even though the cement job is successful, the surrounding ground conditions may still not provide the necessary conductor support (Brechan et al. 2017).

Conductor jetting has been widely used as installation method for deepwater and ultra-deepwater environments because no cement job is required. When jetted in, the conductor support relies only on skin friction between the conductor and the formation. The length of the conductor string is calculated based on soil conditions and the required carrying capacity. A longer conductor will provide higher carrying capacity, as more conductor surface area is exposed to the formation (Prasertamporn 2016).

2.1.2 Conductor Anchor Node (CAN) Technology

An alternative method for installing the conductor is to use Conductor Anchor Node (CAN) technology. This is a new, but already well proven technology developed by the company Neodrill in Norway. The information below is included to give a brief overview of the concept and to illustrate the potential reduction in setting depth that can be achieved by use of the technology.

CAN-technology is a suction anchor based well foundation and it is illustrated in Figure 4. It is designed to provide at the required load bearing capacity as a conventional conductor design, but to be beneficial in terms of cost, safety and reduced wellhead fatigue (Mathis et al. 2017). The dimension of the CAN is adjusted for each specific operation. Normally, the diameter is set to 6m and the length is then adjusted to meet the required load bearing capacity (Mathis et al. 2017). Since the first installation in 2006, conductor anchor nodes have been installed with lengths ranging from 7,5m-17,5m (Neodrill AS 2020).

The basic CAN-design has an integrated guide pipe to ensure vertical installation of the conductor when using methods like jetting or driving. The guide pipe also enables the conductor to be preinstalled in the CAN before shipping it offshore. Preinstallation is done by cementing the 36 inch conductor into the 44,5 inch guide pipe (Mathis et al. 2017). This is referred to as a CAN-ductor design and is illustrated in both Figure 4 and Figure 5. The black stick up in Figure 5 is the 36 inch Low Pressure Wellhead Housing (LPWHH). A benefit of using this installation method is that the cement job quality can be verified onshore, which reduce the wellhead fatigue potential due to lateral movements. The offshore installation process of the conductor anchor node is performed by a vessel in front of rig arrival. This is done by lowering the CAN through the water column on a wire rope and let it self-penetrate some distance into the seabed. An ROV with a pump is then utilized to create a suction pressure inside the cylinder, with the result of increasing the penetration depth to the predetermined level (Mathis et al. 2017).

Figure 4: CAN about to be installed in the Barents Sea in 2018 (Neodrill AS 2020)

Figure 5: Conductor integrated into CAN (Mathis et al. 2017)

The described CAN-ductor design provides several advantages compared to the alternative methods for conductor installation. Cost can be reduced as a lighter and cheaper vessel is used for constructing the conductor section. In this way, drilling of the surface casing section can commence immediately after the drilling vessel arrives at the well site. Pursuant to Aleksandersen and Higgins (2019), the reduction of rig time will typically be in the order of 2-4 days per well. The CAN-ductor can also be installed weeks or even months before the drilling vessel arrives, which adds flexibility in terms of handling harsh weather conditions. Another important aspect is improved safety for rig personnel. The main reason for this is that

handling of large 36 inch conductor tubulars is no longer required by the rig crew. In this way, the probability of crush injuries and falling objects are reduced. In addition, the environmental impact is reduced. Contributing factors for this aspect are removal of the conductor cement job and reduced CO_2 emissions from the operation by 25-45% (Aleksandersen and Higgins 2019).

The CAN-ductor design provides large axial and transverse load capacity, with a short length conductor. This has proven to be a major advantage for constructing horizontal wells in shallow reservoirs, as the CAN provides a solid foundation for shallow kick off point (KOP). Especially in the Barents Sea, thin reservoir layers can be as shallow as 250m BML and where horizontal wells is a necessity for commercial development of these resources (Mathis et al. 2017). This concept is illustrated in Appendix A: Well Trajectory for Shallow Reservoir Layer.

2.1.3 Conductor Shoe Setting Depth

The setting depths of the conductor shoe is of interest to the simulation part of this thesis. An assessment of setting depth for three different conductor designs is therefore presented below. Setting depths are evaluated for a jetted conductor, drilled and cemented conductor and for the CAN-ductor design. The results of the assessment will be evaluated in correlation with the simulations in section 6.3. All data for soil conditions and CAN load capacities are based on field data from the Wisting field in the Barents sea, provided in the paper by Mathis et al. (2017). Table 1 presents the soil condition at shallow depths of the field, while Table 2 presents the capacity of two different conductor designs. The results of the calculations are presented in Table 3, while all assumptions and a more detailed calculation is provided in Appendix B: Calculation of Jetted Conductor Lengths.

Table 1: Soil conditions from geological assessment (Mathis et al. 2017)

Depth [m]	Undrained Shear Strength [KPa]
0,0	6,0
27,0	90,0

Table 2: CAN- dimensions and axial load capacity (Mathis et al. 2017)

CAN- design	OD [m]	Length [m]	Axial Load Capacity [KN]
Short	6,00	7,50	3606
Long	6,00	11,00	7010

Pursuant to Mathis et al. (2017), a drilled and cemented conductor would require a length of at least four joints to provide the same axial load capacity as the long CAN-design in Table 2. By assuming a length of 9,14m (30ft) per conductor joint, the length drilled conductor becomes 36,57m. A third alternative is jetting the conductor and the required length for this string is calculated below. The result of the calculation reflect the required length of a 30 inch jetted conductor in order to provide the same axial load capacity as the CAN designs from Table 2.

Equation 2.1 is provided by Aird (2018) and is used to calculate the jetted conductor length. The equation is based on summarizing the total skin friction acting on the jetted conductor to find the axial load capacity. By rearranging the equation and inserting the CAN-capacities, the required conductor length can be found. In the equation, Q is the axial load capacity, RF is the reduction factor, d_o is the outer diameter of the conductor and cs is the undrained soil shear strength. The integration is performed for depth dz below mud line (BML), from the seabed z_1 to the bottom of the conductor z_2.

$$Q = RF * \pi * d_o * \int_{z_1}^{z_2} cs\, dz \qquad (2.1)$$

Undrained soil strength (cs) is approximated as a linear function in this calculation, where the increase in strength is proportional to the depth BML. The total skin friction is then found in Eq. 2.2, by integrating cs along the length of the conductor from z_1 to z_2. The variables a and b are calculated based on the soil data in Table 1.

$$\int_{z_1}^{z_2} cs\, dz = \int_{z_1}^{z_2} (a \cdot z + b)\, dz = \left[\frac{a}{2} \cdot z^2 + b \cdot z\right]_{z_1}^{z_2} \qquad (2.2)$$

It is assumed that the conductor fully penetrated the seabed during installation, so that z_1 = 0m BML. Eq. 2.3 is then found by inserting the result from Eq. 2.2 into Eq. 2.1 and set it equal to zero. This is a quadratic equation and z_2 is found by using of the quadratic formula. See Appendix B: Calculation of Jetted Conductor Lengths, for detailed calculations.

$$\left(\frac{RF \cdot \pi \cdot d_o \cdot a}{2}\right) \cdot {z_2}^2 + (RF \cdot \pi \cdot d_o \cdot b) \cdot z_2 - Q = 0 \qquad (2.3)$$

The reduction factor RF is dependent on the soil disturbance during installation and is assumed to be 0,8 for this case (Aird 2018). This assumption imply that the soil has regained 80% of the original undrained shear strength. To obtain this value, it is assumed that the conductor is held stationary for some time after installation while the soil regains its shear strength. The results of the calculations in this section are provided in Table 3.

Table 3: Comparison of conductor lengths based on installation methods

CAN- Design	Axial Load Capacity [KN]	CAN-Length [m]	Length Drilled Conductor [m]	Calculated Length Jetted Conductor [m]
Short	3606	7,50	-	32,92
Long	7010	11,00	36,58	46,63

It can be observed that the required lengths for jetted conductors are 32,92m and 46,63m in order to provide the same axial load capacities as the CAN-design. As mentioned earlier, the length of the drilled conductor is based on using four joints with assumed length of 9,14m (30 ft) per joint. The result implies that the depth of the conductor shoe is pushed deeper when a jetted or drilled conductor solution is utilized.

2.1.4 Surface Casing Section

The second section in the well is usually drilled with a 26 inch bit. A 20 inch casing string, often referred to as the surface casing, is then run into the borehole and cemented into place. The string is equipped with an 18 ¾ inch high pressure wellhead on top, which serve as a connection point for later installed blow out preventer (Brechan et al. 2017). Normally, the surface casing defines the deepest set string in the top-hole as the subsequent sections are drilled with the BOP and marine drilling riser installed. However, some wells required a third casing string to be installed while drilling riserless. The additional string is normally installed to overcome shallow geo-hazards, like shallow gas or shallow water flows. These terms describe pressurized and movable fluid in shallow formations, that can cause severe damage and safety concerns if not controlled.

The setting depth for the surface casing are, amongst other factors, dependent on water depth. In shallow waters, the shoe is typically placed at 400-800m (1312-2625ft) BML. For deep waters on the other hand, the string is usually set shallower (Brechan et al. 2017). This trend is caused by the combination of narrow drilling windows, presence of shallow geo-hazards and high cost of non-retrieved drill fluid. The last point is especially relevant if weighted or engineered fluids are required to reach target depth, and the mud cost will therefore increase considerably with section depth. As a result, the casing shoe is typically placed at 244-305m (800-1000ft) BML in deepwater areas, like the Gulf of Mexico (Reksterberg and Kvassheim 2011). However, improved technology for riserless drilling has extended the surface casing setting depth in later years. In some deepwater locations, placing the casing shoe at approximately 610m (2000ft) BML is achievable today (Reksterberg and Kvassheim 2011).

The surface casing has several important functions in the well design. In terms of well integrity, the string has a vital function as an element in the secondary well barrier envelope for the first intermediate hole section. The surface casing has, in combination with its cement, the purpose of isolating the shallow and weak formations in top-hole sections (Stave, Nordas, et al. 2014). In case there exist shallow formations with movable fluids and abnormal pore pressure, the string seals off the wellbore and preventing flow of water or gas from the formation. The string is also an important part of the well foundation. The ability to carry high axial loads from the BOP and deeper run casing strings, is therefore crucial. As a result of these reasons, the surface casing has an important role in maintaining wellbore integrity for the further drilling operation. The priority of a successful installation of the surface casing and

with execution of a high quality cement job, must therefore be emphasized in the well construction process

The surface casing section can be challenging to drill and cement, especially in deepwater and ultra-deepwater locations. Several technology alternatives are therefore utilized to solve drilling challenges and improve efficiency. For instance, some systems include a release and drill ahead assembly like the one described in section 2.1.1. Another option is riserless dual gradient drilling systems, like the RMR-system that is presented in section 3. This system manipulates the bottom hole pressure during drilling and cementing operations, and the surface casing setting depth can therefore be extended many cases.

2.2 Top-hole Cementing Practice

As earlier mentioned, conventional drilling practice is to drill a hole section and to install a casing string into the borehole. Cement is then placed in the annulus to establish integrity between the steel casing and the adjacent formations over time (Brechan et al. 2017). This chapter will give a brief introduction on conventional cement operations, performed from floating drilling vessels. Cement is used for all conventional casing and liner installations, but the focus in thesis will be directed towards cement operations in top-hole sections.

2.2.1 Objective and Requirements

Cement is placed in the annulus between the steel casing and the adjacent formation, both for conventional conductor installation and for the surface casing. The requirements for cementing are regulated by NORSOK-D10 as a part of well integrity. For the surface casing, NORSOK require the string to be cemented inside the conductor or to surface if no conductor is installed (Standards Norway 2004). On the other hand, top-hole strings are normally cemented all the way to the top, meaning that the entire annular volume is filled with cement. This method provides some degree of volume control as cement returns should be observed at wellhead when the job is successful. Lack of returns can indicate downhole problems, like loss of cement to the formation.

When in place, the cement serves several purposes. The main purpose of cementing the conductor string is to prevent drilling fluid from escaping and circulating outside the casing. The surface casing on the other hand, is cemented to protect the well from shallow water

flows and potential gas bearing formations. In addition, the cement will provide a structural connection between the surface casing and the subsurface formation. This structural connection is very important in order to support the considerable weights from the BOP and deeper run casing strings, which will be applied to the surface casing (Brechan et al. 2017). The cement will also create lateral support for the high pressure wellhead, which is placed on top of the surface casing. This is a potential weak point and wellhead fatigue is a common problem caused by force induced motions and vibrations. A high quality cement jo is therefore important for constraining motion and vibrations, resulting in reduced wellhead fatigue.

2.2.2 Cementing Equipment and Displacement Procedure

An extensive set of equipment is stationed on modern drilling vessels with the purpose of mixing and displacing the cement volume. However, the equipment described in this chapter are limited to the basic downhole components, as they are the most relevant for the simulations in the digital model. The conventional way to install a casing string is to lower the string on drill pipe with an installation tool that connects the drill pipe to the casing. There are usually centralizers mounted on the outside of the casing with the purpose of centralizing the string in the wellbore. In this way, the cement can fully surround the string during displacement and therefore improve the integrity. Some operators use two centralizers for each casing joint as a best practice guideline, but the number of centralizers should be adjusted for each section based on well deviation and dog leg severity. Figure 6 illustrates a typical design of a centralizer used on the casing exterior.

The lower end of the casing string is often referred to as the shoe track. It consists of a float shoe, a float collar and one to three casing joints. The purpose of the shoe track is to provide a containment area to entrap fluids that are likely contaminated from the wiping of the top plug down the casing (Brechan et al. 2017). The top of the shoe track is defined by the float collar and it is normally placed one to three joints above the float shoe. During cement displacement, the float collar states the landing point for the cement plugs. The float shoe is placed on the bottom casing joint and helps guiding the casing string when running it into the well. NORSOK-D 010 require at least two float valves to be used in the casing string during installation (Standards Norway 2004). Appendix C: Acceptance Criteria for Casing Float Valves, provides a more detailed explanation of float valve requirements. These backpressure

valves are situated in the float shoe and in the float collar, with the purpose of preventing fluids from entering the casing while running in hole. The valves also prevents flowback of cement into the casing after the cement is placed in the annulus (Brechan et al. 2017). The floats are normally integrated into cement foundations inside the float collar and the float shoe, like illustrated in Figure 7.

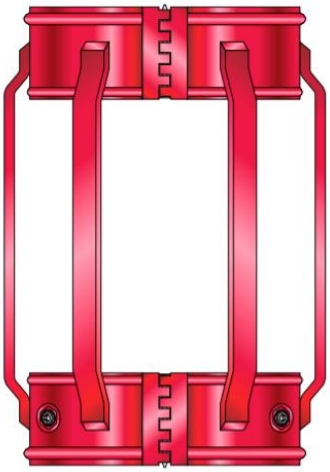

Figure 6: Rigid-bar Centralizer used on casing exterior (Weatherford International 2016)

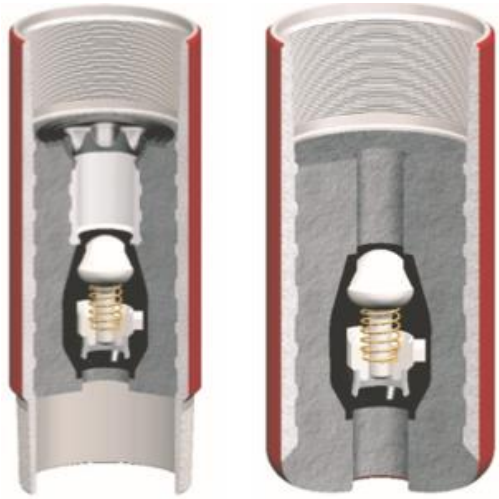

Figure 7: Float collar (left) and float shoe (right) (Weatherford International 2005)

A plug set system is utilized in the cement operation to achieve effective displacement of the cement slurry. The plugs separate the cement from the spacer in front and the cement from the displacement fluid at the tail. This concept and the initial setup for offshore cementing operations from floating vessels are illustrated in Appendix D: Steps in Conventional Cementing. The plugs minimize cement slurry contamination and wipes the inside casing clean of fluids. Several system designs are available on the marked, but a normal composition consists of a ball and a dart, bottom plug and top plug (Brechan et al. 2017). In some system designs, especially for large casing sizes, the ball can be exchanged with a second dart. A plug set system is illustrated in Figure 8, consisting of a top plug (yellow left), bottom plug (red left), top dart (yellow right) and bottom dart (red right). In offshore operations with floating drilling vessels, the plugs are installed in the cement head on drill floor during the operation, while the top and bottom plug are preloaded into the wellhead. This is often referred to as a sub-surface release system (Weatherford International 2013).

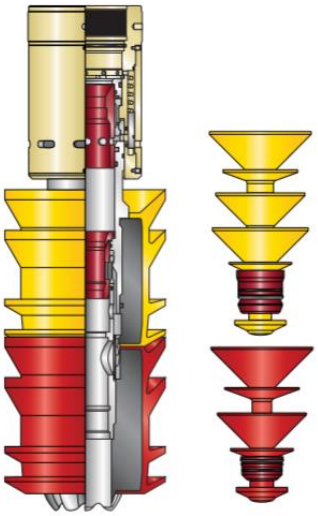

Figure 8: Wiper plugs (left) and darts (right) (Weatherford International 2013)

The conventional procedure for pumping and displacing the cement from the mixing unit to the annular space behind the casing, is illustrated step by step in Appendix D: Steps in Conventional Cementing. The procedure is initiated by pumping a volume of spacer fluid. The spacer has the purpose of separating the drilling mud from the cement slurry, but also to make sure that all surfaces are water wet in case oil based mud (OBM) have been used. When the spacer has been pumped, the bottom dart is dropped from the cement head and followed by the cement volume. The bottom dart lands in the bottom wiper plug situated in the wellhead. Pumping continues and pressure increases until the shear pins in the bottom plug fails and the plug goes in front of the cement. After the whole cement volume has been pumped, the top dart is dropped to release the top wiper plug, which it goes behind the cement (Brechan et al. 2017). In some cases, a single plug system can be utilized for cement displacement and the wiper plug then goes behind the cement.

The bottom plug will land in the float collar when reaching the depth of the shoe track, where the collar provides a solid landing shoulder for the wiper plug. Pumping then continues to break the rupture disc in the bottom plug, so that cement can pass into the shoe track and annular space behind the casing. The top plug lands on top of the bottom plug when the entire cement volume passes the float collar. This is referred to as bumping the plug. The top plug with the inserted dart is solid and seals off the casing string from the shoe track and annular space. As the surface casing are cemented all the way to the top, cement returns should be observed at the wellhead before landing the top plug. After bumping the wiper plugs, the installation tool is activated to seal off the cemented annulus at the wellhead (Brechan et al. 2017).

2.2.3 Design of Cement Slurries and Spacer Fluids

Design of cement slurries and spacer fluids are a large and complex topic. The significance of this topic is rather limited in this case, as only the final properties of the fluid are of importance for the simulations. Therefore, only a brief overview of the different cement additive categories is provided below. The additives exist as liquids or free-flowing powders and are mixed with basic cements to obtain desired slurry properties. Density, viscosity, fluid loss control and curing time are example of slurry properties that can be regulated through the design and mixing process. The following categories of additives are commonly used in cement slurry design (Brechan et al. 2017):

- Accelerators
- Lightweight additives
- Heavyweight additives
- Retarders
- Lost circulation additives
- Fluid loss control
- Dispersants
- Gas control additives

2.2.4 Challenges in Top-Hole Cement Operations

The geological conditions of shallow formations can cause challenges to the cement operation. Some examples of challenging conditions are low fracture gradients and pressurized zones containing movable formation fluids like water or gas. One of the key factors for handling these challenges is to maintain the bottom hole pressure inside the drilling window, but his can become challenging due to the high density of cement slurries. When the cement slurry moves into the annulus, the lower density mud is displaced, and bottom hole pressure will gradually increase. Depending on the slurry density, this increase can be significant and result in lost circulation if the fracture pressure is exceeded. Cement volumes will then be lost to the formation, which can cause unwanted consequences like zonal isolation problems and loss of integrity.

Flow of formation fluids through the cement column is another challenge that may occur in shallow formations. This exchange of fluid between the annulus and formation can cause channeling in the cement and therefore zonal isolation problems. Pursuant to Stave, Nordas, et al. (2014), wells have started to flow even after the cement is in place, either due to loss of cement to the formation or due to lost hydrostatic pressure when the cement sets.

There are several measures available for controlling the downhole pressure during cement operations. One option for reducing the bottom hole pressure is to use low density slurry

design, like foam cement. This will reduce the difference in hydrostatic pressure as mud is displaced by cement in the annulus. Another available measure is to use a manage pressure cementing (MPC) system, which utilize a subsea installed pump to manipulate the downhole pressure. The same system can be utilized for preventing flow of formation fluids into the cement column, after the cement is in place. This technique will be further explained in section 3.2.4, together with design and capacities of the MPC system.

2.3 Basic Wave Theory

The wave type relevant for this master thesis is named mechanical waves but is often referred to as pressure waves, when propagating in fluids. This wave type transfer energy through particle oscillations in a medium. The movement of one particle is transferred to the neighboring particle through viscous forces, and the wave is therefore able to propagate trough the medium (Ormestad 2018).

The initial oscillation of the particles is caused by an external force acting on the medium. For the phenomenon studied in this thesis, the external force is a result of breaking the shear pins and releasing the wiper plug. The compressed fluid in the landing string then expands to equalize pressure and the wiper plug is pushed down in a rapid motion. This motion is believed to induce a pressure pulse, propagating through the system by the same principle as the pressure wave described above.

A pressure wave propagating through a fluid is categorized as a longitudinal wave, because particle oscillation takes place along the same direction as wave propagation (Ormestad 2018). Propagation of a longitudinal wave is simulated in this thesis and factors that affect the amplitude of the wave are therefore of great interest. The pressure amplitude reflects the energy of the wave and a loss of energy will correspondingly reduce the pressure amplitude (Ormestad 2018). Loss of energy are related to several factors. For instance, energy is lost to friction as the moving particles are exposed to frictional forces along the walls of the fluid conduits. Also, energy is lost to fluid mixing and flow separation when the wave passes geometrical irregularities on the propagation path (Cengel and Cimbala 2014).

3 Riserless Mud Recovery (RMR) System

Riserless mud recovery (RMR) is a type of dual gradient drilling system used within top-hole drilling and cementing operations. The technology is based on using a subsea pump module to lift the mix of drill fluid and cuttings from the seabed up to the drilling vessel. In this way, the system eliminates discharge to sea and enables dual gradient drilling by use of weighted and engineered muds (Stave, Fossli, et al. 2014). The system can also be used during cement operations and it is then referred to as a manage pressure cementing (MPC) system.
A representation of the MPC- system was implemented into the digital model, with the purpose of evaluating if pressure waves from the wellbore could affect the subsea installed equipment. This chapter will provide detailed knowledge on RMR- and MPC- systems designed for shallower water depths. The information in this chapter is based on the system from the company Enhanced Drilling, because this design is adequately described in literature.

3.1 System Components

The riserless mud recovery system is illustrated in Figure 9. This type of system configuration has been utilized for more than 350 wells (Enhanced Drilling 2020) and in water depths up to 854m (Claudey et al. 2016). The system consists of the following key components:

1. Suction Module (SMO)
2. Subsea Pump Module (SPM)
3. Umbilical and Umbilical Winch (UW)
4. Office and Tool Container (OTC)
5. Power and Control Container (CC)
6. Mud Return Line (MRL)

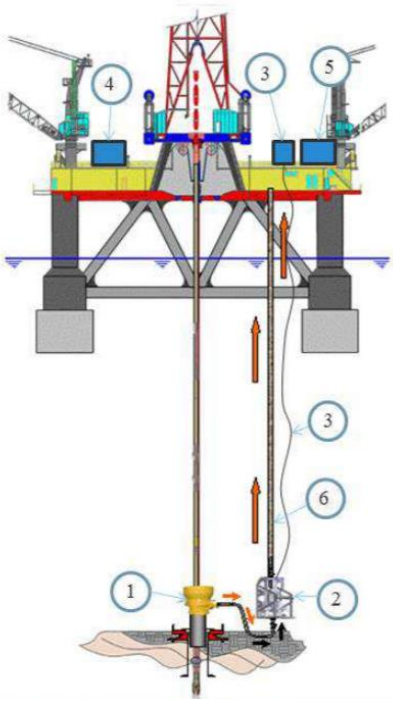

Figure 9: Setup for the riserless mud recovery system (Stave, Nordas, et al. 2014)

3.1.1 Suction Module

The suction module function as a collection chamber for mud and cuttings as they exit the wellbore. It is usually installed on top of the low pressure wellhead housing with an ROV friendly connection point for the suction hose. Figure 10 and Figure 11 illustrate the SMO. Redundant lighted cameras and a high accuracy pressure transducer are used to continuously monitor the mud level inside the chamber (Smith et al. 2010). The RMR operator controls the system from the drilling vessel. Once drilling is initiated and the mud level reaches the desired level, automatic mode is activated by the RRM operator. The system then analyze data from the pressure transducer and adjust the pump speed of the subsea pump module to maintain a constant mud level in the chamber (Stave, Fossli, et al. 2014).

In some environmentally friendly areas, like the Barents Sea, RMR technology can be utilized for eliminating discharge to the marine environment during top hole drilling operations. When using the RMR system to drill the conductor section, a spud base mounted SMO is utilized. The spud base has skirts that are lowered into the seabed before drilling is initiated. There also exist a spud base design with a collection chamber outside the SMO. This design is used to collect accidental spills from the SMO (Stave, Fossli, et al. 2014). Regardless of base type, mud and cuttings are transported from the SMO to the subsea pump module by a flexible suction hose.

The suction module has an open top design, which results in fluid contact between the mud and the sea water. An open top design implicates that the system cannot be pressurized. In the early phase of using this technology, it was believed that a rotating sealing element was needed to avoid spills of mud to the marine environment. A low pressure sealing element, designed for up to 5 bar pressure difference, was therefore used during a field trial with the drilling vessel Erik Raude. Later experience shows that the RMR system can be used successfully with an open mud cap, without spills of drill fluid to sea (Stave, Fossli, et al. 2014). The open cap version has become the industry standard and it is illustrated in Figure 10 and Figure 11(Enhanced Drilling 2020).

Figure 10: SMO mud level monitored by cameras and lights (Smith et al. 2010)

Figure 11: Suction module (Enhanced Drilling 2020)

3.1.2 Subsea Pump Module

The subsea pump module (SPM) lifts the returns of drill fluid and cuttings from the seabed back to the drilling vessel. The setup used for shallower waters consist of a seabed installed SPM connected to the suction module by a flexible suction hose. The pumps are driven by electrical motors, which receive electrical power and control signals from the control container (CC) through an umbilical line (Claudey et al. 2016). The subsea pump module is also equipped with a diverter valve, which provide circulation options during the cement job. For instance, excess cement can be discharged to sea without entering the return line and shaker system. This is obtained by closing the return line valve and open the diverter valve when cement is verified at the wellhead. The diverter valve also enables flushing of the return line with sea water, while staying connected to the wellhead (Elahifar 2020). The subsea pump module and the valves are illustrated in Figure 12 and Figure 13.

The required head capacity for pumping mud back to surface is dependent on water depth and mud properties. To meet the required head capacity for a certain water depth, pumps and motors are normally installed in staged configuration (Claudey et al. 2016). For instance, a three staged subsea pump configuration provided the sufficient head capacity for drilling a 26 inch section in 854m water depth. This particular operations took place on the Norwegian Continental Shelf in 2016 and it was the deepest deployment of the seabed installed SPM at that time (Claudey et al. 2016). In order to provide an idea of size and capacity, the three-staged pump mentioned above had a weight of approximately 10 metric tons and could be configurated to yield a discharge pressure of 130 bar (Claudey et al. 2016).

The capacity of handling cuttings is a criterion for the subsea pump module and disc pump technology is used for this purpose. The technology can handle solid particles of up to 2 inches (5,08cm) in diameter and with minimal damage of the cuttings (Smith et al. 2010). The efficiency of the pumps is mainly dependent on two factors, the drill fluid viscosity, and the internal clearance around the disc in the pump. Since the pump must be able to handle cuttings there will always be a compromise between pump efficiency and cuttings tolerance (Reksterberg and Kvassheim 2011). Today, a common efficiency value for these pumps will be in the interval of 50-60 % (Elahifar 2020).

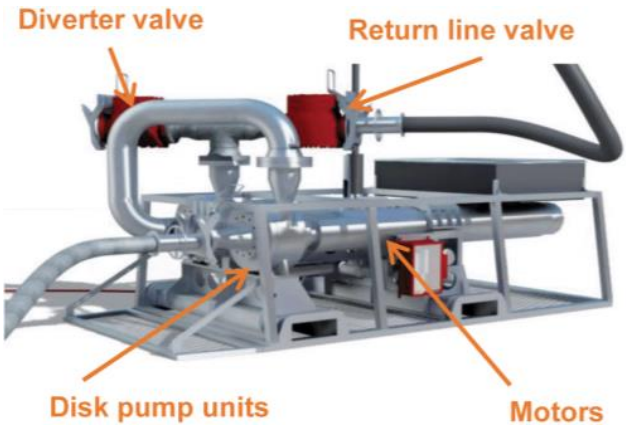

Figure 12: Subsea pump module
(Claudey et al. 2016)

Figure 13: Staged pump configuration
(Claudey et al. 2016)

3.1.3 Mud Return Line

The mud return line usually consists of a 6 inch heavy duty hose, made up in 15m sections (Thorogood et al. 2007). It provides return of drill fluid and cuttings back to the drilling vessel. The heavy duty hose is joined by quick connect couplings and it is reinforced with load bearing wires, stung from integral lugs on each connector (Thorogood et al. 2007). In some cases, hard piping has been utilized as MRL to create a more robust alternative. For instance, a 8 5/8 inch casing pipe has successfully been used as a mud return line in water depth 854m (Claudey et al. 2016). There are also examples of using hard piping only through the splash zone, in order to avoid the hose from colliding into the rig in harsh weather (Elahifar 2020).

The MRL has a dedicated handling platform installed on side of the vessel. It includes a handling system for deployment and retrieval of the return line, but also a hang off shoulder to

take weight of the return line when it is deployed. In addition, the handling platform contains a landing manifold, where the return line is the connected during operation. Hard piping then unites the landing platform manifold and the shale shaker header box (Thorogood et al. 2007). In this way, mud returns can enter the mud system on the drilling vessel and be reconditioned.

3.1.4 Umbilical and Winch

The umbilical line provides electrical power and communication between the subsea pump module and the control container. The umbilical is also used for deployment and retrieval of the SPM over the side of the drilling vessel. This operation is performed by using an umbilical winch, located on the side of the vessel. A second umbilical line connects the subsea pump module to the suction module, providing power and communications to lights, cameras and the pressure transducer on the SMO (Thorogood et al. 2007).

3.1.5 Deck Installed Containers

The RMR system requires two container units to be installed on the deck of the drilling vessel. Both units are illustrated in Figure 9. The office and tool container function as a work area for the crew and as a station for monitoring the health of the system. It also serves as a workshop, with storage space for spare parts. Both container units are pressurized (Thorogood et al. 2007).

The control container house the communication and power equipment used to control the subsea pump module (Smith et al. 2010). Important components in this container are the variable speed drive, transformer, and control system. The variable speed drive controls the pump rate of the SPM, while the transformers provide high voltage power for the subsea equipment. The purpose of the control system is to provides an interface between the drilling vessel and the RMR system. It monitors income data from the SPM and the SMO, and then adjust the system performance to maintain the stable mud level in the suction module. The operator can control the system from a dedicated computer located in the drillers cabin. In addition, the system has two emergency shut down bottoms, one located in the drillers cabin and one in the control container (Thorogood et al. 2007).

3.1.6 Installation Procedure

The whole RMR system can be transported to the drilling vessel by a supply vessel, and then lifted onboard before the drilling operation is initiated. In this way, most of the setup can be performed outside the critical time frame. The tasks performed in critical time are installation of the suction module, deployment of the subsea pump module and subsea connection of components. The total duration of these tasks are approximately 4-6 hours (Elahifar 2020).

During installation, the SMO is deployed through the moon pool using drill pipe or a tugger winch with guidelines. It is then clamped to the low pressure well head housing. The subsea pump module (SPM) is the lowered over the side of the vessel using an umbilical winch. An ROV connects the suction line and umbilical line from the SPM to the SMO, as a last part of the subsea setup (Enhanced Drilling 2019). In case the system is used for drilling the conductor section as well, then a spud base will be installed before drilling is initiated. The different spud base designs were described in section 3.1.1 and the design is selected based on the requirements for each specific well.

3.2 Primary Drivers for Using Riserless Mud Recovery Systems

This section will present some of the primary drivers for using the riserless mud recovery system. Most drivers are concentrated on solving difficult drilling challenges and to improve both drilling efficiency and safety (Stave, Nordas, et al. 2014). Manage pressure cementing, which take part in the later presented simulations, will also be described in this section. The information below is important in order to understand how the RMR system is utilized to overcome difficult challenges in top-hole drilling and cementing operations.

3.2.1 Improved Well Control

The RMR system is a closed loop system, which provides several advantages in terms of well control. Compared to the conventional method of using seawater as drill fluid, the system enables weighted and engineered mud to be used. In this way, control of downhole pressure is improved and it can be ensured that the wellbore hydrostatic pressure is always in overbalance with the formation pore pressure (Stave, Nordas, et al. 2014). The risk of encountering uncontrolled flow from permeable and abnormal pressured formations, are therefore minimized. In addition, mud types containing fluid loss material can be utilized to build a filter cake on the borehole wall with the RMR system. This will further reduce the loss and flow potential (Stave, Nordas, et al. 2014).

Pursuant to NORSOK-D-010 point (4.2.3.7), volume control of fluid shall be maintained at all times when the fluid is a well barrier (Standards Norway 2004). During conventional top-hole drilling, sea water is used as the only barrier and the methods used for volume control are inaccurate. The RMR system on the other hand, introduce accurate volume control during top-hole drilling operations. Variation in flow rates are effectively detected by the subsea pumps and control system, which enables early kick and loss detection. In addition, the system enables reliable flow checks to be performed in order to control the stability of the well (Stave, Nordas, et al. 2014).

Early influx detection is especially important for successful handling of shallow gas kicks. The volume control capacity of the RMR system is therefore beneficial, as it increases the chance of detecting influxes while the gas is still down hole. Compared to the conventional method, where an ROV is used for seabed observation, gas volumes are first detected when emerged at the seabed. During this time, significant gas volumes may have entered the wellbore, making it harder to dynamically kill the well (Stave, Nordas, et al. 2014).

3.2.2 Increased Setting Depth of Surface Casing

The riserless mud recovery system provides dual gradient drilling (DGD) capacity, which is beneficial in terms of manipulating the pressure regime in the wellbore. Figure 14 illustrates the concept, where the bottom hole pressure is a result of hydrostatic pressure from two fluid columns of different density. The upper part of dual gradient consists of the sea water column that stretches down to the wellhead interface. The lower part consists of weighted mud inside the wellbore, which is usually denser than seawater. Dual gradient capacity normally extends the depth at which the surface casing must be set to avoid exceeding the fracture pressure (Claudey et al. 2016). Figure 14 illustrates the potential increase in surface casing setting depth, based on a given case of pore pressure and fracture pressure gradients. The extended setting depth can in some cases reduce the need of a third casing string in the top-hole section, which is beneficial for drilling efficiency and cost.

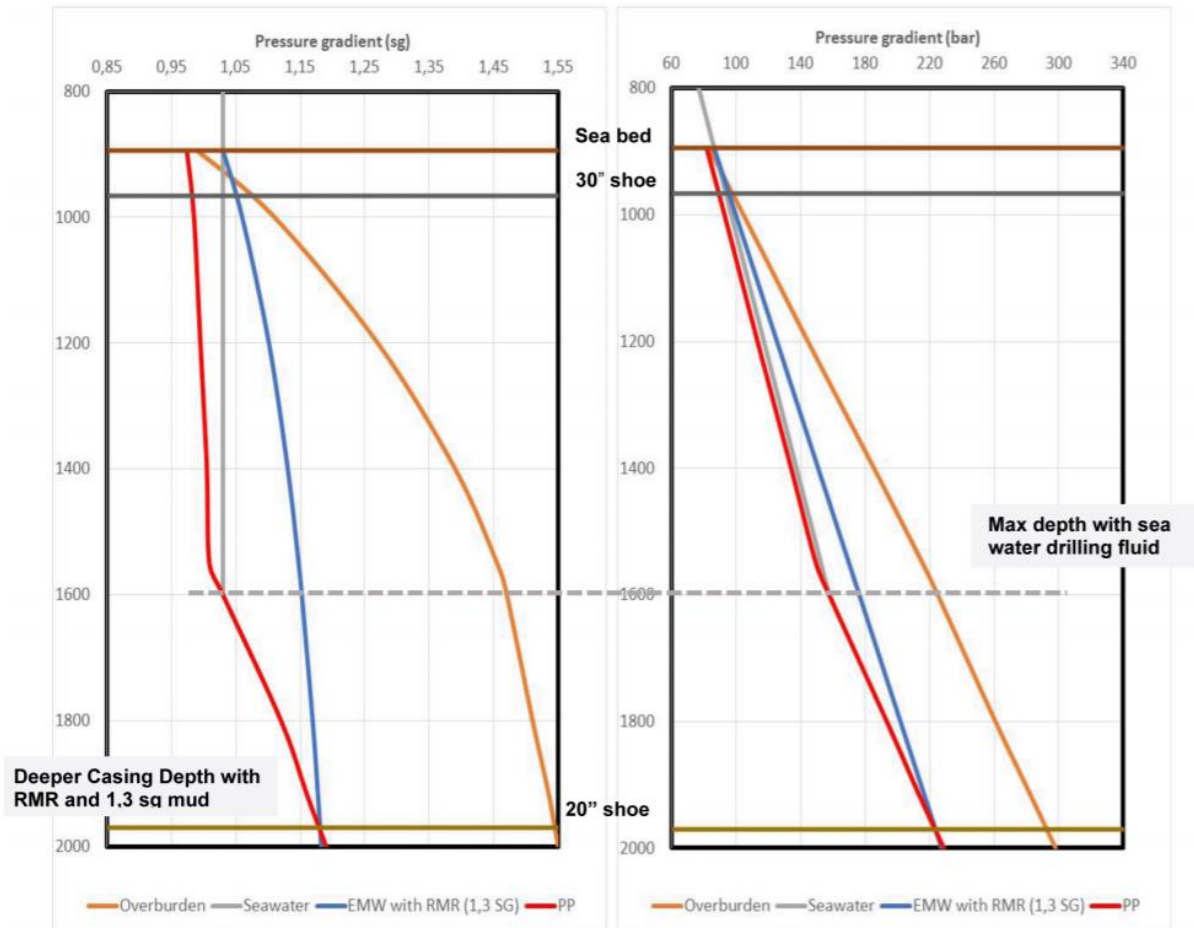

Figure 14: Effect of a dual gradient drilling system in terms of increased surface casing setting depth (Claudey et al. 2016)

3.2.3 Reduced Impact on the Marine Environment

Even though most of the primary drivers are related to solving difficult drilling challenges, there is also an environmental driver for using this technology. The RMR system reduces the environmental impact on the marine environment, by removing disposal of drill fluid and cuttings to the sea. Normally, sea water or water based fluids are utilized for drilling top-hole sections. The environmental impact on the surroundings are therefore limited, but some areas may require special measures like in the case described below.

Exploration for hydrocarbons are sometimes performed in vicinity to areas with vulnerable ecosystems, like cold water corals and spawning ground for fish. In these areas, access may only be granted if the operator complies with a zero discharge philosophy. A field example that describes this scenario is the Toutatis well, which was drilled by the operator Wintershall DEA in 2019. The well was located about 8km from the sensitive Træna-revet on the Norwegian Continental Shelf and great measures was executed by the operator in order to be granted access (Miljødirektoratet 2019). The RMR system may in these cases become a requirement in order to explore and economically develop these resources, both now and in the future.

3.2.4 Manage Pressure Cementing

Manage pressure cementing (MPC) is a spin off technology from the drilling application of riserless mud recovery systems (Stave, Nordas, et al. 2014). The system setup is the same, except that the subsea pump module is connected to a different valve on the SMO. For MPC purposes, the subsea pump module is used for managing the annulus pressure during cement displacement. The system is illustrated in Figure 15, where the MPC- valves are marked with red circles. These valves were also implemented in the digital model and can be observed on the block scheme in Appendix F: Overview Digital Model. During cement displacement, one of these valves is connected to the suction hose, while the other one stays closed. In the moment of breaking the shear pins and releasing the wiper plug, the closed valve is opened in order to let potential pressure pulse pass without obstruction.

The MPC- system provides at least three types of applications. The first application is to regulate the wellbore pressure during cement displacement in the annulus. For this purpose, the pump speed is increased to lift more fluid weight in the return line and by this reduce the pressure at top of the annulus. This pressure reduction will also be seen by the downhole

formation. When the cement level rises in the annulus, the pump is speeded up in accordance to a pre-determined step down pressure schedule, resulting in constant pressure for critical zones in the well (Stave, Nordas, et al. 2014). In this way, the risk of fracturing the formation is reduced. When cement returns are verified at the subsea pump module, the MPC- valve connected to the suction line is closed and the suction hose is disconnected. The purpose of this procedure is to seal off the well from ambient pressure and to entrap the reduced pressure in the annulus during the curing process of the cement (Stave, Nordas, et al. 2014).

The second area of application is cement verification at the wellhead, which can be performed with high degree of certainty compared to conventional methods. For this application, the pump holds a constant speed until cement is detected at the pump module. The MPC- valve to the sea is then opened to enable cross head circulation and flushing of the lines (Elahifar 2020). This ensures that the annulus between the conductor and surface casing is filled to the top with cement, which is beneficial for preventing wellhead fatigue during the life of the well.

The third application is to apply backpressure on the annulus after cement returns have been verified, with the purpose of preventing flow from pressurized zones. This is performed by filling the return line to the top with sea water, then close the MPC- valve to sea and shut off the pump. An additional backpressure of approximately 2,5 bar is then obtained due to the distance from the sea surface to the MRL landing station. By monitoring the fluid level in the MRL, loss or fluid influxes can be detected after the cement is in place (Elahifar 2020).

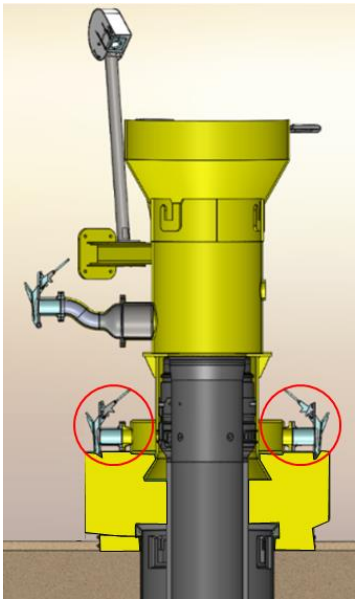

Figure 15: Manage pressure cementing (MPC) system (Elahifar 2020).

4 Simulations

A simulation model was built in Matlab to enable further investigation of pressure and flow effects in top-hole cementing operations. The model was utilized for simulating transient pressure events and to evaluate the energy loss for a migrating pressure pulse. This chapter presents the constructed model in detail and it describes fundamental equations, assumptions and the approach for implementing non-Newtonian rheology models. Also, the chapter includes a description of the physical case that was examined and simulated in the model. The results of the simulation are presented in Chapter 5 and further discussed in Chapter 6.

4.1 Background for Simulations

The background for the simulations is a desire to explore the pressure pulse phenomenon in greater detail and to evaluate the potential risks that the pulse may represent. A pressure pulse is in this context defined as a time dependent change in pressure from a compressed fluid volume, which is generated by a force acting on the fluid system. For the simulations, primary attention was given to the pressure pulse from releasing the wiper plug. An important aspect was to investigate how the magnitude of the propagating pressure pulse was affected by the physical properties of the system. The technique used for this purpose was to measure the pressure at critical points in the well and then alter system properties one by one. In this way, important knowledge about the energy loss across system components could be developed.

The motivation for constructing the model and performing the simulations, was to figure out if the pressure pulse can cause damage to the formation or to the equipment. Formation damage may occur if the wellbore pressure exceeds the fracture gradient, leading to lost circulation problems. The subsequent result may be a total loss of the well, which generates impacts on both safety and economy. Subsea equipment like valves, pipes and hoses may also be affected by the pressure pulse. In the case where pressure exceeds the rated capacity of the equipment, component failure is expected. The consequences of component failure will often be operational delays, increased costs and potential safety concerns. Therefore, investigation of the pressure pulse effects is of high interest to avoid challenges and hazards during top-hole cementing operations.

4.2 Case Description

The case to be investigated, is the pressure transient that emerge from releasing a wiper plug for cement displacement in a surface casing. Figure 16 illustrates the simulated case at initial conditions. As described in section 2.2.2, the wiper plugs are used for separating the cement volume from spacer in front and displacement fluid at the tail. The top and bottom plug are situated inside the wellhead and they are released when the darts arrive through the landing string. In the simulations, the pressure pulse from releasing the bottom plug was investigated.

When the bottom dart lands in the bottom wiper plug, pumping continues until the differential pressure across the plug reaches the plug launch pressure. The magnitude of the launch pressure is determined by the number and strength of the shear pins integrated in the wiper plug. When launch pressure is obtained across the plug, the shear pins will break, and the plug moves downwards in a rapid motion. This will create a pulse of compressed fluid, often referred to as a pressure wave or longitudinal wave, that migrates downwards in the casing. At bottom hole, the energy will to some extent be reflected and travel upwards through the annulus before it arrives at the wellhead. Depending on pressure amplitude, this wave can potentially cause damage to the formation or to subsea installed equipment as it travels through the system. The presence of a subsea installed MPC- system was therefore implemented into the simulated case illustrated in Figure 16. In the simulations, pressure at bottom hole and pressure at the MPC- valves were measured. The sketch below is also presented in Appendix E: Illustration of the Physical Case, because it may then be easily compared to the digital model illustrated in Appendix F: Overview Digital Model.

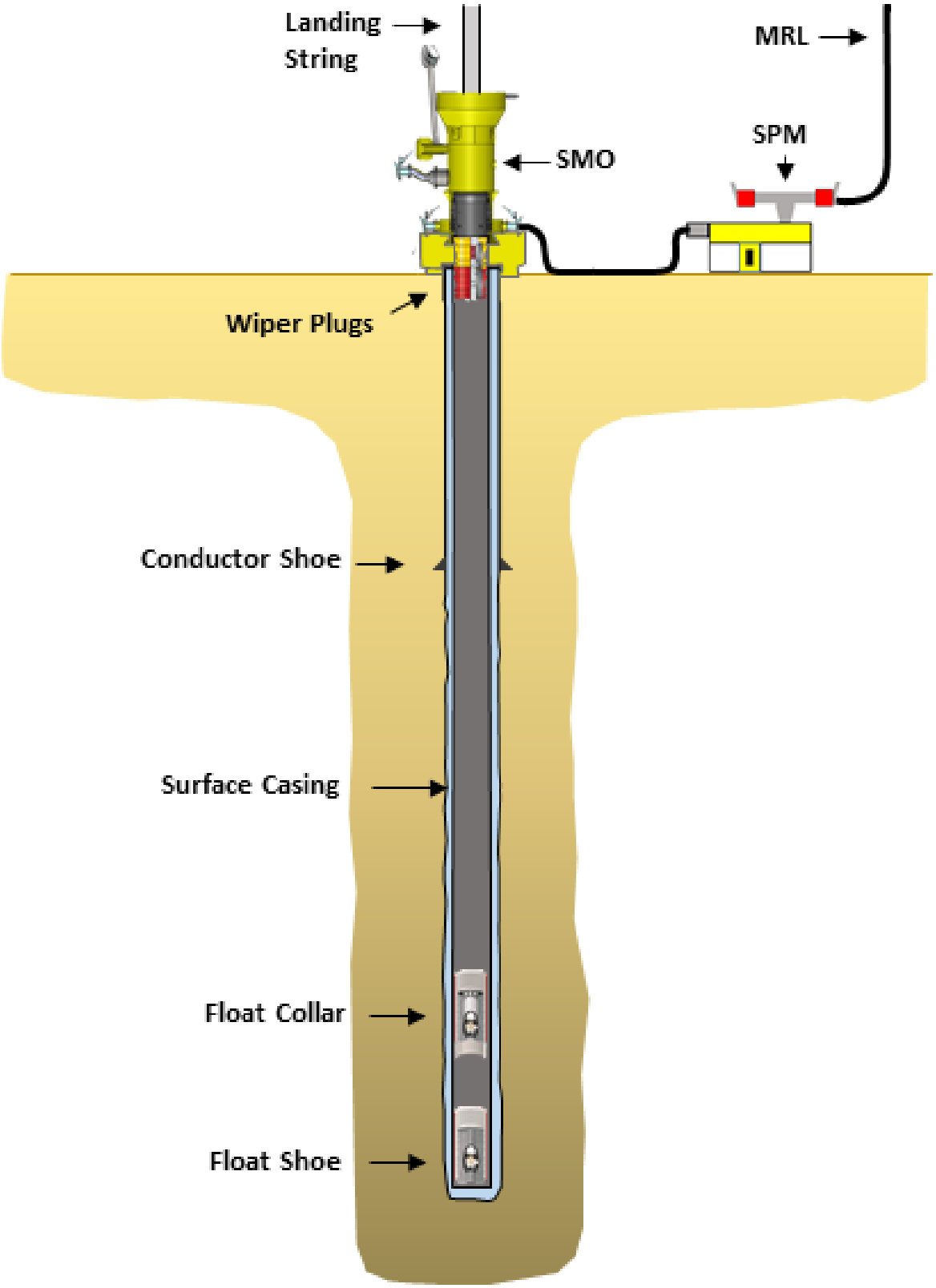

Figure 16: Sketch of the physical case that was modelled (Made by the author, with cuts from (Weatherford International 2005), (Weatherford International 2013) and (Elahifar 2020)

4.3 Software

Model construction and simulations were performed in the software Matlab R2020a. Matlab has an advanced tool package named Simscape Fluids, which is a part of the Simulink product family. This tool package was utilized for modelling the physical system and to perform fluid simulations. Simscape Fluids offers several categories of fluid simulations and the category named thermal liquid (TL) were chosen for this case. The reason for choosing this option, was that this library provides the most favorable prerequisites for simulating transient pressure in top-hole systems. Some of these prerequisites are flexible options for model construction, numerical computation capacity and options for data visualization and analysis.

The Simscape software is based on block schemes and the scheme for the constructed model is illustrated in Appendix F: Overview Digital Model. The blocks represent the different physical components of the top-hole system, but also inputs and output signals. All blocks used in the model were premade by the Simscape software and existed in block libraries. When building the model, blocks were chosen and coupled together, creating the specific top-hole system presented in Figure 16. A traditional Matlab program code was also developed in order supply the Simscape model with the correct input parameters and initial conditions. The program code is further discussed in section 4.8 and the input variables are presented in section 4.7.

4.4 Discretization and Fundamental Equations

The core system of the Simscape fluid model contains differential and algebraic equations, which are computed by a numerical solver in terms of unknown variables (The MathWorks Inc. 2020b). The equations are defined in the representative blocks and in domain definition files. When the blocks are connected in the model scheme, the software assembles the system of equations during compilation and then solves them for each time step of the simulation (The MathWorks Inc. 2020b). Since the fundamental equations are block specific, it will not be favorable to present them all in this chapter. The presentation of fundamental equations and method of discretization are therefore based on the block named pipe (TL). This block models all liquid filled conduits in the system like casing strings and annular conduits, and which contributes with important effects in the simulations.

Discretization of the model is a necessity in order to use a numerical solver on the system of equations. For conduits modelled by the pipe (TL) block, the number of discretized segments is dependent on the time scale for which pressure pulse travels through the pipe (The MathWorks Inc. 2020a). In compliance with the Nyquist sampling theorem, the number of pipe segments is found by solving for N in Eq. 4.1. The theorem is also illustrated in Figure 17 and it states that at least two computational nodes are required within one wavelength in order to capture an elementary sinusoidal disturbance (The MathWorks Inc. 2020a). In Eq. 4.1, N defines the number of required pipe segments, L is the total length of the pipe, c is the speed sound in the fluid and f is the frequency of the disturbance. Dividing the modelled pipes into a number of ten segments, was found to provided sufficient resolution and enabled accurate interpretation of results.

$$\frac{c}{f} = 2 \cdot \frac{L}{N} \tag{4.1}$$

The most fundamental equations for computational fluid dynamics describes conservation of mass, conservation of momentum and conservation of energy (Cengel and Cimbala 2014). These equations are implemented in all Simscape Fluids blocks describing the physical system. The equations are valid under the assumption that the system retains a constant volume. All implemented blocks were configured as rigid in the model and the assumption of constant system volume is therefore valid. An overview of a pipe segment with ports A and B is shown in Figure 18.

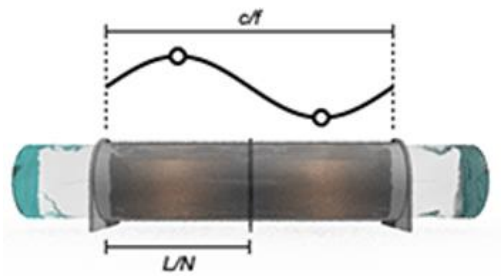

Figure 17: Illustration of the Nyquist sampling theorem (The MathWorks Inc. 2020a)

Figure 18: Discretized pipe with port A and port B (The MathWorks Inc. 2020a)

The equations for conservation of mass, momentum and energy are presented as balances below. The mass balance for a pipe segment is given in Eq. 4.2. In the equation, $\dot{m}_A$ and $\dot{m}_B$ denotes the mass flow through port A and port B. Subscript I denotes that the variable represents an internal fluid property of the system. Thus, ρ_I denotes the density of the fluid, while $\dot{p}_I$ and $\dot{T}_I$ are the rate of change for temperature and pressure in the fluid. Further, V is the internal pipe volume, β_I represents the bulk modulus and α_I the thermal expansion coefficient of the fluid (The MathWorks Inc. 2020a). Right hand side of equation 4.2 represents the change in fluid mass inside the pipe as a function of pressure and temperature. Only the effect of pressure was investigated in this thesis, since the system was treated as perfectly isolated. This is further explained in section 4.6.3.

$$\dot{m}_A + \dot{m}_B = \rho_I V \left(\frac{\dot{p}_I}{\beta_I} - \alpha_I \dot{T}_I \right) \tag{4.2}$$

The next equation to be presented is conservation of momentum and it is split over two control volumes, each representing half of the pipe volume. This is necessary for capturing effects from fluid compressibility and fluid inertia. The control volumes are referred to by subscription A and B, where subscript A describes the control volume adjacent to port A and B the control volume adjacent to port B. Inlet and outlet surfaces of the control volumes are assumed perpendicular to the pipe centerline (The MathWorks Inc. 2020a).

The momentum balance is given in Eq. 4.3 and in Eq. 4.4, where P_A and P_B represent pressure at port A and B. The term g denotes the gravitational acceleration, Δz the vertical elevation from port A to port B, L is the pipe length and S is the cross-sectional flow area of the pipe. $P_{F,A}$ and $P_{F,B}$ are the pressure loss due to friction along the pipe walls, which is further described in the section 4.5.2 and 4.5.3. Due to fluid compressibility, the internal liquid pressure P_I can vary nonlinearly along the pipe. Therefore, both Eq. 4.3 and Eq. 4.4. are required in order to compute the pressure development at an internal computational node, denoted I. The fluid inertia concept states that a change in flow momentum is not instantaneous. This effect is captured in the right-most term, where $\ddot{m}_A$ and $\ddot{m}_B$ represent the rate at which mass flow rate changes in control volume A and B (The MathWorks Inc. 2020a).

$$P_A - P_I = P_{F,A} + \rho_I g \frac{\Delta z}{2} + \frac{\ddot{m}_A}{S}\frac{L}{2} \tag{4.3}$$

$$P_B - P_I = P_{F,B} - \rho_I g \frac{\Delta z}{2} + \frac{\ddot{m}_A}{S}\frac{L}{2} \tag{4.4}$$

The energy balance is presented in Eq. 4.5 and it describes the rate of energy accumulation in the conduit. Term $\dot{E}_I$ is the energy accumulation rate, while ϕ_A and ϕ_B is the energy flow rate through port A and B. ϕ_H is the heat flow rate between the thermal liquid and the pipe wall, which is neglected in compliance with the explanation in section 4.6.3. The right-most term in Eq. 4.5 is the potential energy term and it is computed using the mass flow rate $\dot{m}_I$ at an internal computational node. $\dot{m}_I$ is calculated as an average in Eq. 4.6, based on the established flow rates at the pipe ports (The MathWorks Inc. 2020a).

$$\dot{E}_I = \phi_A + \phi_B + \phi_H - \dot{m}_I g \Delta z \tag{4.5}$$

$$\dot{m}_I = \left(\frac{\dot{m}_A + \dot{m}_B}{2}\right) \tag{4.6}$$

The accumulation term $\dot{E}_I$ can also be expressed as the total energy of the internal fluid, using the specific energy as described in Eq. 4.7. In the equation, t denotes time, P is pressure, T is temperature and u is the specific internal energy of the fluid (The MathWorks Inc. 2020a). The right-side term inside the parenthesis in Eq. 4.7, describes the change in internal energy as a function of temperature and pressure. Like with the equations for mass and momentum, the effect of temperature changes will not be investigated as the system is assumed to hold a constant temperature.

$$\dot{E}_I = \rho_I V \left(\frac{du}{dP}\frac{dP}{dt} + \frac{du}{dT}\frac{dT}{dt}\right)_I \tag{4.7}$$

4.5 Hydraulics

Several types of drill fluid and cement slurries can be used during construction of the top-hole sections. Each fluid type has characteristic properties that will affect the development and dampening of the pressure pulse. Models for fluid rheology and frictional pressure losses were therefore constructed and implemented into the simulations. In this way, the model enables examination of fluid effects on the pressure wave development. This section provides information on fluid types and basic equations used for describing the hydraulic effects.

4.5.1 Rheology and Flow Regime

Fluids are categorized in terms of rheology, which describes how the fluid deforms and how flow resistance develops. Rheology is normally defined by the shear stress τ and shear rate $\dot{\gamma}$ (Guo and Liu 2011). This thesis deals with two categories of fluids, namely Newtonian and non-Newtonian fluids. Sea water is treated as a Newtonian fluid, which means that the shear stress is proportional to the shear rate. In other words, the flow resistance increases linearly with flow deformation (Guo and Liu 2011). This fluid is commonly used during conventional top hole drilling, especially in shallower waters. The alternative is to use non-Newtonian fluids, which is the category of most slurries and engineered drill fluids. This category of drill fluids is used in top-hole sections under application of RMR technology and are therefore of great interest for the simulations. In non-Newtonian fluids, shear stress is not directly proportional to the shear rate. Different models are therefore used for describing the rheology of Non-Newtonian fluids, like the Bingham plastic model or the power law model, depending on the fluid behavior (Guo and Liu 2011).

The engineered drill fluids used for top-hole drilling are water based. They normally consist of sea water and clay particles like bentonite, with the purpose of providing filter cake capacities, additional weight, and gel strength. The advantages provided by these characteristics were explained in section 3.2. Pursuant to Guo and Liu (2011), compositions of sea water and clay normally comply with plastic behavior and the Bingham plastic model was therefore selected for describing the rheology of non-Newtonian fluids in this thesis. The friction loss model for Newtonian fluids and non-Newtonian fluids are presented in greater detail in section 4.5.2 and section 4.5.3.

The flow regime in the conduits is determined by the Reynolds number Re, which is a function of flow rate and conduit geometry. Flow with Re < 2000 is treated as laminar flow and flow with Re> 4000 as turbulent flow (The MathWorks Inc. 2020a). The frictional pressure drop is higher for turbulent flow compared to laminar flow, because chaotic flow pattern results in high energy consumption and therefore correspondingly high head loss in turbulent flow (Brechan et al. 2017). This is illustrated in Figure 19, where it can be observed that pressure loss increases exponentially with flow rate in the turbulent flow regime. The figure also illustrates the correlation between flow regime, Reynolds number and pressure drop. The zone in between laminar and turbulent flow is referred to as the transition zone.

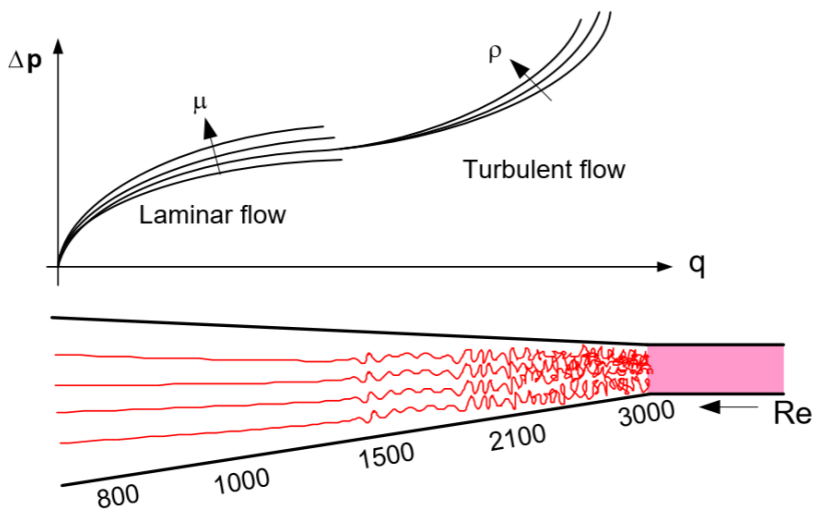

Figure 19: Reynolds number vs. flow and pressure drop
(Brechan et al. 2017)

In the Simscape model, the Reynolds number for Newtonian fluids is calculated by Eq. 4.8. The term $\dot{m}_j$ denotes the mass rate, D_h is the hydraulic diameter, S is the cross sectional flow area and μ_I is the dynamic viscosity. Subscript j denotes the control volume, either the one adjacent to port A or the one to port B (The MathWorks Inc. 2020a).

$$Re = \frac{\dot{m}_j D_h}{\mu_I S} \tag{4.8}$$

Simscape Fluids only offer circular pipe geometry. Therefore, the concept of hydraulic diameter D_h is used for calculating the Reynolds number. D_h is defined by Eq. 4.9, where p is the wetted perimeter and A_c is the cross sectional area of the pipe (Cengel and Cimbala 2014). The hydraulic diameter concept was used for approximating the annular conduit by a circular pipe, and with a pipe diameter that consider the extra friction in the annulus. From Eq 4.9, the hydraulic diameter between the casing and the wellbore becomes $D_h = d_{Wellbore} - d_{Casing\ OD}$.

$$D_h = \frac{4A_c}{p} \tag{4.9}$$

4.5.2 Friction Loss Model Newtonian Fluids

A model for calculating the frictional pressure drop in Newtonian fluids is provided by the Simscape software. This model was utilized for simulations where sea water was utilized as drill fluid. The fundamental equation for calculating the frictional pressure loss in conduits, is provided in Eq. 4.10. It is based on the Darcy-Weisbach equation and is valid for both laminar and turbulent flow (The MathWorks Inc. 2020a). The term $f_{D,j}$ is the Darcy friction factor for the control volume and L is the length of the pipe.

$$P_{F,j} = f_{D,j}\frac{1}{4}\frac{L\dot{m}_j|\dot{m}_j|}{\rho_I D_h S^2} \tag{4.10}$$

The Darcy friction factor $f_{D,j}$ is calculated from Eq. 4.11 or Eq. 4.12, depending on the flow regime. Equation 4.11 is valid for laminar flow, where λ is the shape factor of the pipe. A shape factor of 64 represents a circular pipe and was utilized both for the casing and the annulus approximation in this thesis (The MathWorks Inc. 2020a). The Haaland correlation in Equation 4.12 is utilized for turbulent flow, where the friction factor also depends on the diameter and the absolute pipe roughness ε. The correlation is empirical (The MathWorks Inc. 2020a).

$$f_{D,j} = \frac{\lambda}{Re_j} \tag{4.11}$$

$$\frac{1}{\sqrt{f_{D,j}}} = -1{,}8log\left[\left(\frac{\epsilon/D_h}{3{,}7}\right)^{1.11} + \frac{6.9}{Re_j}\right] \tag{4.12}$$

4.5.3 Friction Loss Model for non-Newtonian Fluids

The Simscape Fluid software is not designed to calculate the frictional pressure loss for non-Newtonian fluids directly. A model for pressure loss was therefore constructed in separate Matlab scripts. The scripts implement the calculated results into the Simscape model as nominal pressure drops across components. Further description of the Matlab scrips are provided in section 4.8. The equations selected for calculating the pressure drop are based on the Bingham plastic model. This follows the assumption from section 4.5.1, that the rheology of non-Newtonian fluids comply with the Bingham plastic behavior in this thesis.

The Bingham plastic model describes a fluid which require a certain magnitude of shear stress before it deforms. This magnitude is called the yield point and it approximates the gel strength of the fluid. In other words, the fluid maintain zero shear rate until the shear stress exceeds a certain magnitude. Once mobilized, the relationship between the shear stress and shear rate is linear (Guo and Liu 2011). The rheology of Bingham plastic fluids is described in Eq. 4.13 and in Figure 20, where τ is the shear stress, τ_γ is the yield shear stress (yield point), μ_p is the plastic viscosity and $\dot{\gamma}$ is the shear rate.

$$\tau = \tau_\gamma + \mu_p\dot{\gamma} \tag{4.13}$$

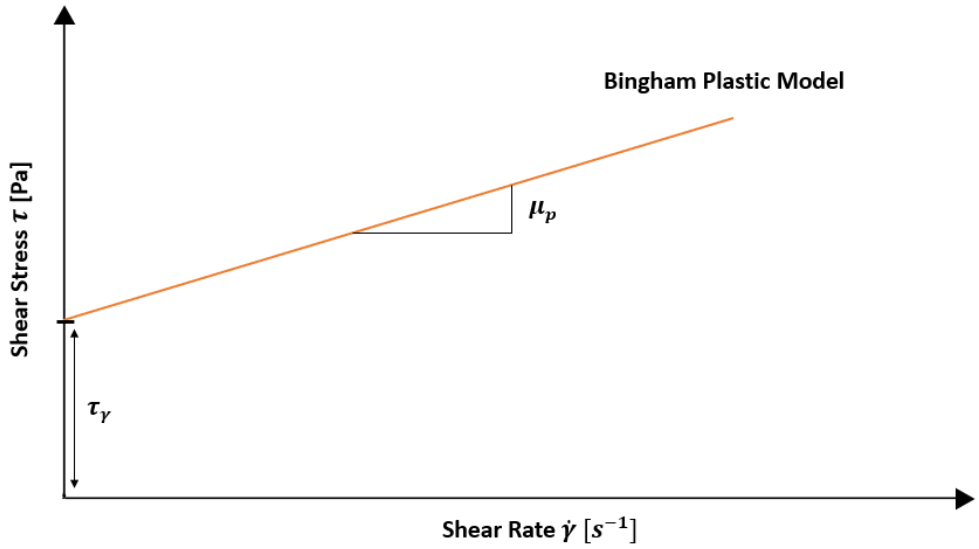

Figure 20: Bingham plastic model (made by the author)

The equations below were utilized in the model to calculate the frictional pressure loss for non-Newtonian fluids. Equations 4.14 through 4.23 were provided by Guo and Liu (2011) and stated in SI units. The equations are utilized under the assumption of smooth pipe, which is valid for most rotary drilling applications involving relatively viscous drilling fluids (Guo and Liu 2011). First step in calculating the frictional pressure loss is to determine the flow regime based the on Reynolds number. Equation 4.14 provides the Reynolds number for a circular pipe, while Eq. 4.15 provides the Reynolds number for the annulus.

$$Re = \frac{\rho \bar{v} d}{\mu_a} \tag{4.14}$$

$$Re = 0.816 \cdot \frac{\rho \bar{v}(d_2 - d_1)}{\mu_a} \tag{4.15}$$

In the equations above, ρ is the fluid density, $\bar{v}$ is the average fluid velocity, d is the diameter of the pipe and μ_a is the apparent viscosity. The term $0.186(d_2 - d_1)$ in Eq. 4.15 describes the equivalent circular diameter of a slot representation of the annulus, used for calculating the Reynolds number for Bingham plastic fluids (Guo and Liu 2011). The term $(d_2 - d_1)$ described the hydraulic diameter of the annulus, where d_2 is the outer diameter and d_1 is the inner diameter of the annulus. The average fluid velocity in a circular pipe is provided by Eq. 4.16 and for the annulus in Eq. 4.17, where q is the flow rate.

$$\bar{v} = \frac{q}{\frac{\pi}{4} d^2} \tag{4.16}$$

$$\bar{v} = \frac{q}{\frac{\pi}{4} ({d_2}^2 - {d_1}^2)} \tag{4.17}$$

The apparent viscosity for Bingham plastic fluids is defined by Eq. 4.18 for pipe flow and by Eq. 4.19 for annular flow. This is a modification that accounts for the plastic viscosity and the yield point of the fluid (Guo and Liu 2011).

$$\mu_a = \mu_p + \frac{0{,}1669 \tau_\gamma d}{\bar{v}} \tag{4.18}$$

$$\mu_a = \mu_p + \frac{0{,}1253 \tau_\gamma (d_2 - d_1)}{\bar{v}} \tag{4.19}$$

After calculating the Reynolds number and choosing a flow regime, the equations below were utilized for calculating the frictional pressure loss in the conduits. As with the Newtonian fluids, the flow is assumed laminar for Re < 2000 and turbulent for Re > 4000. For laminar flow, pressure drop is described by Eq. 4.20 for pipes and by Eq. 4.21 for the annulus. For turbulent flow, pressure drop is described by Eq.4.22 for pipes and by Eq. 4.23 for the annulus. In the equations below, ΔL describes the length of the conduit.

$$\Delta P_f = \left(\frac{\mu_p \bar{v}}{31{,}33 d^2} + \frac{\tau_\gamma}{187{,}5 d} \right) \Delta L \tag{4.20}$$

$$\Delta P_f = \left[\frac{\mu_p \bar{v}}{20{,}88 (d_2 - d_1)^2} + \frac{\tau_\gamma}{166{,}7 (d_2 - d_1)} \right] \Delta L \tag{4.21}$$

$$\Delta P_f = \frac{\rho^{0{,}75} \bar{v}^{\,1{,}75} \mu_p^{0{,}25}}{6320 d^{1{,}25}} \Delta L \tag{4.22}$$

$$\Delta P_f = \frac{\rho^{0{,}75} \bar{v}^{\,1{,}75} \mu_p^{0{,}25}}{4901 (d_2 - d_1)^{1{,}25}} \Delta L \tag{4.23}$$

4.6 Wellbore Pressure Regime

It is important to control the wellbore pressure regime and to keep the pressure inside the drilling window during operations. The consequence of exceeding the limits may be fluid influxes and wellbore instability at the lower end or fracturing and lost circulation at the higher end. The wellbore pressure consists of three components, namely the hydrostatic pressure, circulation pressure and transient pressure. This also apply for the wellbore pressure in the digital model and the pressure components are briefly explained below.

4.6.1 Equivalent Circulating Density (ECD)

The bottom hole pressure is dependent on the weight of the hydrostatic column. In addition, the pressure will increase when circulating due to the frictional pressure losses in the annulus. Together, the two components constitute the Equivalent Circulating Density (ECD), which describes the actual bottom hole pressure during circulation. The ECD is described by Eq. 4.24, where ρ_m is the mud density, g is the gravity constant, z is the height of the fluid column and ΔP_{ann} is the frictional pressure loss in the annulus (Reksterberg and Kvassheim 2011). In the digital model, the effect from annular pressure loss is embodied into the momentum equation, presented in Eq. 4.3 and Eq. 4.4. The term ΔP_{ann} is believed to be small in the simulations, due to the low displacement rate of cement and no slurry in the annulus.

$$P_{ECD} = \rho_m g z + \Delta P_{ann} \tag{4.24}$$

4.6.2 Transient Pressure and Signal Generator

The transient pressure component is a time dependent change in pressure. In the case of this thesis, the transient component is a pressure pulse moving through the system. To simulate initiation of this pressure pulse, a signal generator was created and added to the model. This component generates a Simulink signal, based on a user defined function. The signal generator is illustrated in Figure 21 and it provides flexibility in terms of shape and magnitude of the desired pressure signal. Input variables for the signal generator are time and wiper plug release pressure. The output is a Simulink based signal, that is converted to a physical signal, before it is inserted as pressure in the Simscape (physical) part of the model.

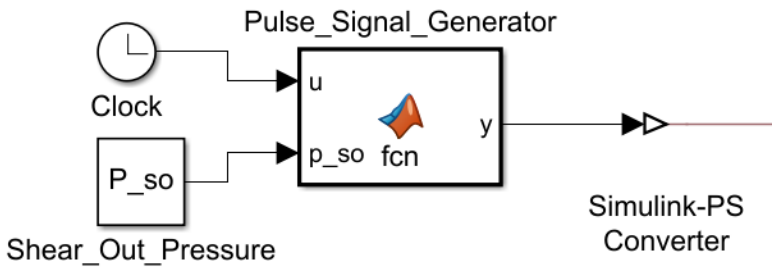

Figure 21: Pressure signal generator
(cut from model)

In the simulations, the generated signal represents the pressure pulse from releasing the wiper plug. As earlier mentioned, the wiper plug moves downward in a rapid motion when breaking the shear pins. This motion has similarities with a positive piston displacement in a cylinder and Eq. 4.25 was therefore chosen as an approximation for the real physical signal. The equation is time dependent and describes a simple symmetric pressure pulse, based on the input variables P_{lp} , a and b. The term P_{lp} describes the amplitude of the signal and it is set equal to the wiper plug launch pressure. This assumption indicate that all the energy stored across the wiper plug, will be transferred into the fluid as pressure when releasing the plug. Validity of this assumption is further discussed in section 6.2. The variable a and b describe the shape of the generated signal, and which were adjusted to approximate the physical signal from the wiper plug motion. The assumed values for the input parameters are presented in Table 4 and the output signal in Figure 22.

$$P(t) = P_{lp} \cdot e^{-\left(\frac{t-a}{b}\right)^2} \tag{4.25}$$

Table 4: Input parameters for Eq. (4.25)

Variable	Value	[Unit]
$\boldsymbol{P_{lp}}$	1000 / 68.95	[psi / bar]
a	1,5	[unitless]
b	0,5	[unitless]

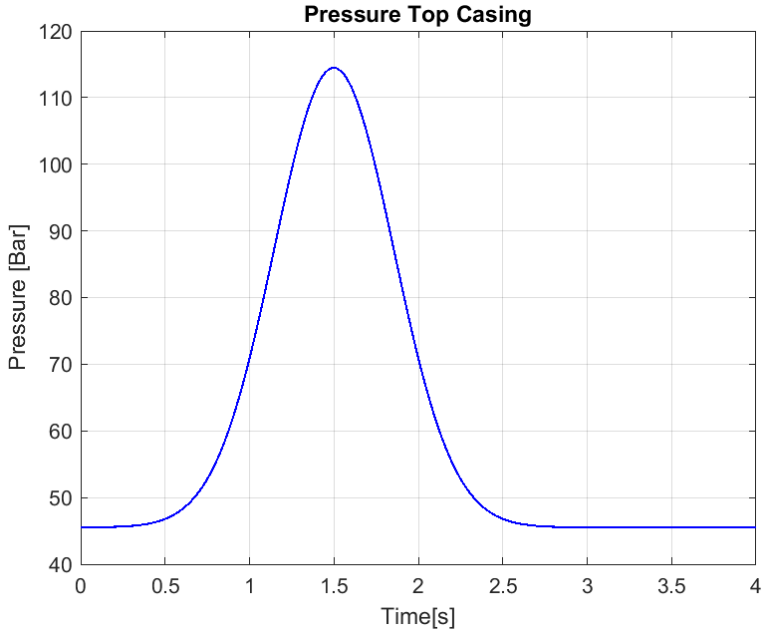

Figure 22: Pressure pulse signal from signal generator (cut from model)

4.6.3 Thermal Effects

The simulations performed in this master thesis neglect thermal effects and the temperature of the system is assumed to be constant. This implies that fluid density and viscosity is not affected by changes in temperature. In a real situation, the liquid in the system is exposed to changes in thermal energy from pipe friction, convection in the fluid and conduction from the surrounding environment. The energy balance, provided in Eq. 4.5, accounts for this heat exchange with the surroundings through the conduction term ϕ_H . However, ϕ_H is neglected in the model as all the components are supplied with perfect insulating capacities, resulting in no heat exchange with the environment. This assumption is applied to reduce the complexity of the model and the number of input parameters.

The top-hole sections consist of large diameter wellbores and with casing strings that contain large fluid volumes. Great amounts of thermal energy from friction and conduction would therefore be required to change the fluid temperature considerably. Also, the geothermal gradient in shallow formations will not provide large temperature differences with the wellbore fluid in most cases, leading to less conduction with the surrounding environment. It is therefore believed that the assumption of constant fluid temperature can be justified without significant impacts on the simulated results. The fluid temperature in the system is set to 281,15K (8°C), which is an approximation based on North-Sea conditions.

4.7 Assumptions

4.7.1 Digital Representation of Float Valves

Geometrical irregularities are a known source of energy loss for moving fluid particles. A digital representation of the spring actuated float valve in the float collar and float shoe, was therefore important to implement in the model. Difficulties were experienced in this process, as no adequate blocks were available for this type of component. Several blocks were tested but later rejected due to numerical instability and violation of model limitations. The solution for digital representation became use of gate valves, with implemented discharge coefficients to approximate a more reliable value for the pressure loss.

Gate valves have different geometry than spring actuated float valves, like those illustrated in Figure 7. Therefore, the concept of discharge coefficients C_d was used for approximating a more representative pressure loss across the valves. C_d is a correction factor with a positive value less than one, that accounts for frictional effects across geometrical irregularities (Cengel and Cimbala 2014). The value of C_d is determined experimentally, but representative data for the float valves was not available to the author. It was therefore decided to use correlations with known geometries.

An orifice plate can correlate to the inlet geometry of the spring actuated float valve. For an orifice plate, the value of C_d is approximately 0,61 (Cengel and Cimbala 2014). The float valves on the other hand, are equipped with an internal mechanism which is assumed to produce even more frictional effects. Therefore, a discharge coefficient of 0,5 was selected to represent the float valves in the digital model. Due to the uncertainty associated with this value, a separate set of simulations were performed with the purpose of investigating the pressure drop effect from altering the value of C_d. The results of the simulations are presented in section 5.2.3 and the validation of the gate valve approximation is further discussed in section 6.2.

4.7.2 Hydraulics and Fluid Properties

Three different fluids were simulated in the digital model with the purpose of studying fluid effects on the pressure wave. The fluid type and properties are presented in Table 5 below. Density and viscosity of the water based muds (WBM) are based on clay content. It was assumed that WBM #2 has a higher clay content than WBM #1, and therefore higher density and viscosity. Generic data for yield point and plastic viscosity for clay contents in water based muds, were provided by (Elahifar 2020). The other properties of the fluids are generic and based on typical characteristic found in literature.

Table 5: Fluid properties used in model

Property [unit]	Sea Water	WBM #1	WBM #2
Density [kg/m^3]	1030	1150	1250
Bulk Modulus [GPa]	2,34	2,34	2,34
Dynamic Viscosity [Pa-s]	0,00149	--	--
Yield Point [Pa]	---	5,7456	7,7566
Plastic Viscosity [Pa-s]	---	0,014	0,019

It is further assumed the following for the hydraulic model:

- The Bingham plastic model applies for calculations of frictional pressure loss for the non-Newtonian fluids
- Flow due to displacement of cement is fully developed in the casing and in the annulus before arrival of the pressure pulse
- Smooth pipe assumption applies for all calculations involving water based muds
- Fluid is compressible
- Fluid responds to fluid inertia
- The system is perfectly isolated, and the fluid holds a constant temperature of 281,15K (8°C)
- Drill fluid properties are valid for the entire fluid volume. This implies that only one fluid is assumed to exist in the system, neglecting presence of slurry and spacer fluids
- The entire fluid volume exists in liquid phase

4.7.3 Pressure Pulse

- It is assumed that all energy from shearing out he wiper plug is transferred to the fluid. The initial magnitude of the pressure pulse is therefore assumed to be equal to the differential pressure required to break the shear pins in the wiper plug
- The shape of the pressure pulse from releasing the wiper plug follows Eq 4.25.
- The pressure pulse is exposed to perfect reflection at bottom hole without loss of momentum or energy

4.7.4 Well and Equipment

Table 6 provides the assumed properties for the base case that was illustrated in Figure 16. The properties are based on common operational characteristics found on the Norwegian Continental Shelf (NCS). Dimensions of float equipment are collected from Weatherford International (2005) and wiper plug launch pressure from Weatherford International (2013). The base case was created in order to provide a data set that could be utilized as a base for comparison. Effects from altering the parameters in Table 6 will be presented in Chapter 5. In the table below, the term Rotary Kelly Bushing (RKB) describes the level of the drill floor on the rig, while True Vertical Depth (TVD) describes the vertical distance to the drill floor.

Table 6: Parameters for base case simulations

Description [unit]	Value	Description [unit]	Value
Water Depth [m]	450	Surface Casing OD [in]	20
Sea to RKB [m]	25	Surface Casing ID [in]	18,73
First Section TVD [m]	525	Surface Casing Length [m]	400
Second Section TVD [m]	875	Length Track Length [m]	24
First Section Hole Size [in]	36	Float Collar ID [in]	3,25
Second Section Hole size [in]	26	Float Shoe ID [in]	3,25
Conductor OD [in]	30	Plug Launch Pressure [bar]	68,95
Conductor ID [in]	28	SMO Valve ID [in]	6
Conductor length [m]	50	Abs. Pipe Roughness [mm]	0,015

It is further assumed the following for the well:

- All surfaces in contact with the fluid volume are rigid so that the volume of the system stays constant
- All sections in the wellbore are vertical
- Length of rat hole is neglected, implying that casing setting depth equals the drilled depth of the section
- Centralizer placements comply with best practice, resulting in perfect casing centralization in the wellbore and a symmetric annulus
- The valves in the float collar and float shoe are fully open during the entire simulation. This is a simplification with purpose of making the simulations run smoother. In the model, a cement slurry displacement rate of 400 l/min is utilized and it is therefore believed that the assumption can be justified.
- The pressure applied to the annulus through the MPC- valve is equal to the hydrostatic pressure at the seabed. This means that the subsea pump module is assumed to lift the hydrostatic pressure difference between the sea water column and mud column in the return line. This assumption was applied because no cement volume enters the annulus during the simulations and a downhole pressure reduction is therefore not required at that time. The dual hydrostatic pressure gradient is still present under this assumption.

4.8 Explanation of the Program Code

The Matlab model consists of five different files. One run script, three Matlab functions and one Simulink file that contains the Simscape model. The simulations are run from the file named Sim_Run_Script.m. This file takes input parameters, insert them into the Simscape model, runs the simulation and delivers the result as output values. During this process, the function Fluid_Parameters.m provides the fluid input parameters, while the functions dp_nnf_casing.m and dp_nnf_annular.m calculates frictional pressure losses, when simulating non-Newtonian fluids. The Sim_Run_Script.m file consists of several sections and the sections are explained in chronological order below.

- **Input Data:** All input parameters receptive for alternation are defined by the user in this section. The user must also select a fluid type for the simulation. This is done by setting the parameter fluid_type equal to 1, 2 or 3. Fluid type 1 is sea water, type 2 is WBM #1 and type 3 is WBM #2, all with properties from Table 5.
- **Oilfield to SI-Units Converter:** Converts all inputs values expressed in oilfield-units into SI-units.
- **Retrieving Fluid Parameters**: Calls the function Fluid_Parameters.m, which retrieve the respective fluid parameters based on the selected fluid type
- **Area Calculations:** Calculates cross sectional areas for all conduits in the system
- **Down Hole Pressure Calculations:** Calculates the initial pressure conditions in the system
- **Load Model:** Loads the Simscape model
- **Insert Fluid Data and pressure Drop:** If sea water is selected as drill fluid, this section inserts the fluid properties directly into the Simscape model. The model then calculates the frictional pressure losses from the equations presented in section 4.5.2. If a water based mud is selected as drill fluid, this section calls the functions dp_nnf_casing.m and dp_nnf_annular.m, which calculates the frictional pressure drop in the conduits based on the equations presented in section 4.5.3. These functions calculate the pressure drop across fluid conduits for many flow rates and returns the pressure drop in table format. The tables are then inserted into the Simulink model, where the software selects the pressure drop values that best represents the actual flow in each of the fluid conduits.

- **Insert Component Data into Model:** This section inserts the necessary parameters from the Sim_Run_Script.m into the respective blocks in the Simscape model.
- **Simulation:** Performs the simulations and returns the results from all sensors. The results are returned in array format, logged with time versus pressure or volumetric flow rate.
- **Organization and plotting:** Organize the result into arrays with names representing the sensor location in the system. The results are then plotted with time vs. pressure or with time vs. volumetric flow rate.
- **Results into Table:** This section organizes the results from the simulation into table format, in order to make it easy for the user to extract results.

The Simscape model file is named Pressure_Pulse_Model.slx. It consists of a block scheme with blocks representing the physical components of the system. An overview of the model is presented in Appendix F: Overview Digital Model and descriptions for each block are provided in Appendix G: Block Descriptions. Use of a powerful computer is recommended for running the simulations.

5 Results

The results presented in this chapter describes pressure at multiple locations in the well. Table and graph format are used for displaying the simulated result. Pressure and flow values are measured by sensors in the digital model. Placement of these sensors were strategic, with the aim of investigating pressure and flow development at important locations in the well. The table descriptions are explained below and the reader is further recommended to look at Appendix F: Overview Digital Model, for a visual explanation. The sensor locations are as followed:

- **Top Casing:** Inside the uppermost joint of the surface casing, right below the wiper plug release point.
- **Top Shoe Track:** Inside the last joint of the casing string, right above the float collar and shoe track.
- **Bottom Hole**: In the open hole at bottom of the well, right below the shoe of the surface casing.
- **Conductor Shoe:** Inside the annulus at the depth of the conductor shoe.
- **Top Annulus:** Top of the annulus, at the MPC- inlet valve to the suction line. This point is located right below the high pressure wellhead housing.

The pressure measurements from the simulations are described as:

- **Initial:** Describes the initial pressure at the location, before releasing the wiper plug. This pressure represents the components from hydrostatic pressure and from circulation.
- **Pressure Max:** Describes the maximum pressure at the location during the simulation. This pressure represents the total pressure, which includes all three pressure components.
- **Pressure Min:** Describes the minimum pressure at the location during the simulation. This pressure represents the total pressure, which includes all three pressure components.
- **Pulse Magnitude:** Describes the magnitude of the pressure pulse itself, without contributions from the hydrostatic column and circulation.
- **Pulse Dampening:** Describes how much energy the pressure pulse has lost to the surroundings up to that point in the well. The energy loss is represented as a pressure loss.

5.1 Base Case

The results of the base case simulations are presented below. All assumptions for these simulations were presented in section 4.7. Table 7 below describes the results from using sea water as drill fluid, while Table 8 and Table 9 represents use of WBM #1 and WBM #2. Pressure development at bottom hole and at the conductor shoe for the different cases are illustrated in Figure 23 through Figure 28.

The results from the simulations state that the formation will be exposed to an additional pressure of 10,21 - 11,28 bar from the pulse, depending on the drill fluid. The additional pressure at the conductor shoe is estimated to be in between 1,04 - 1,24 bar and 0,32 bar at the top of the annulus. From the bottom row of the tables, it can also be observed that the largest pressure drop is simulated to take place across the shoe track. The simulations estimate this pressure drop to constitute a portion of 81,3% - 83,3%, depending on the type of drill fluid. The measured values for pressure do not follow all the expected trends. For instance, the pressure pulse is measured to the same magnitude at the conductor shoe for all three fluids. This does not make sense based on the differences in fluid viscosity, which should induce dissimilarities. The validity of these results and the potential sources of error are further discussed in Chapter 6.

Table 7: Wellbore pressure development for sea water

	Top Casing [bar]	Top Shoe Track [bar]	Bottom Hole [bar]	Conductor Shoe [bar]	Top Annulus [bar]
Initial	45,53	83,52	85,89	50,52	45,47
Pressure Max	114,46	150,94	96,09	51,57	45,79
Pressure Min	45,52	83,52	80,15	50,10	45,47
Pulse Magnitude	68,93	67,42	10,21	1,04	0,32
Pulse Dampening	0	1,51	58,73	67,89	68,61

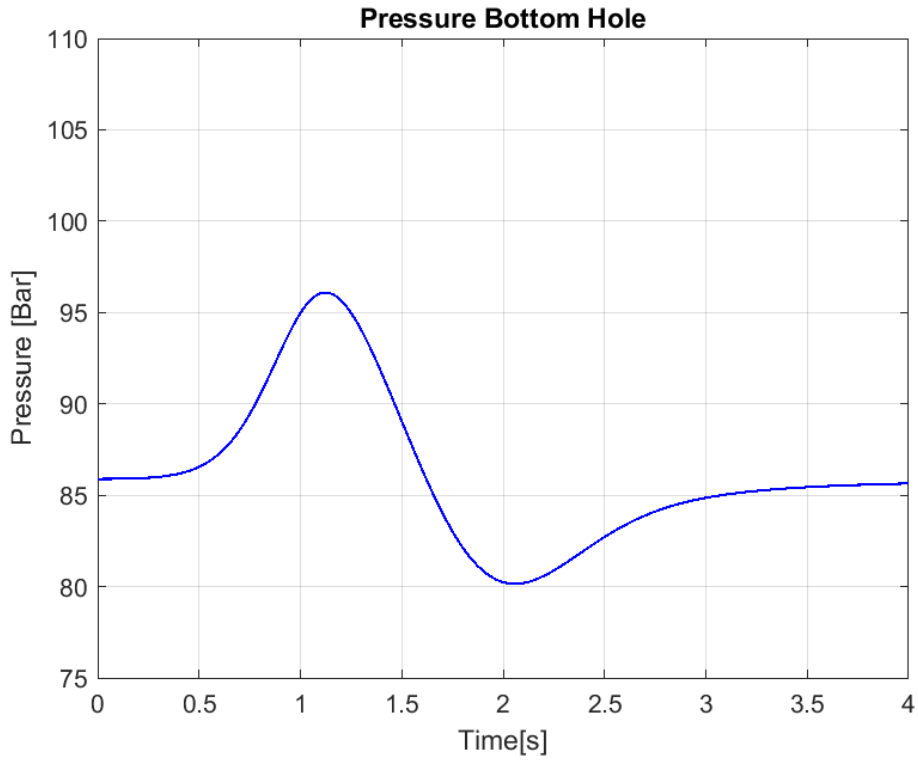

Figure 23: Pressure at bottom hole. Base case with sea water as drill fluid

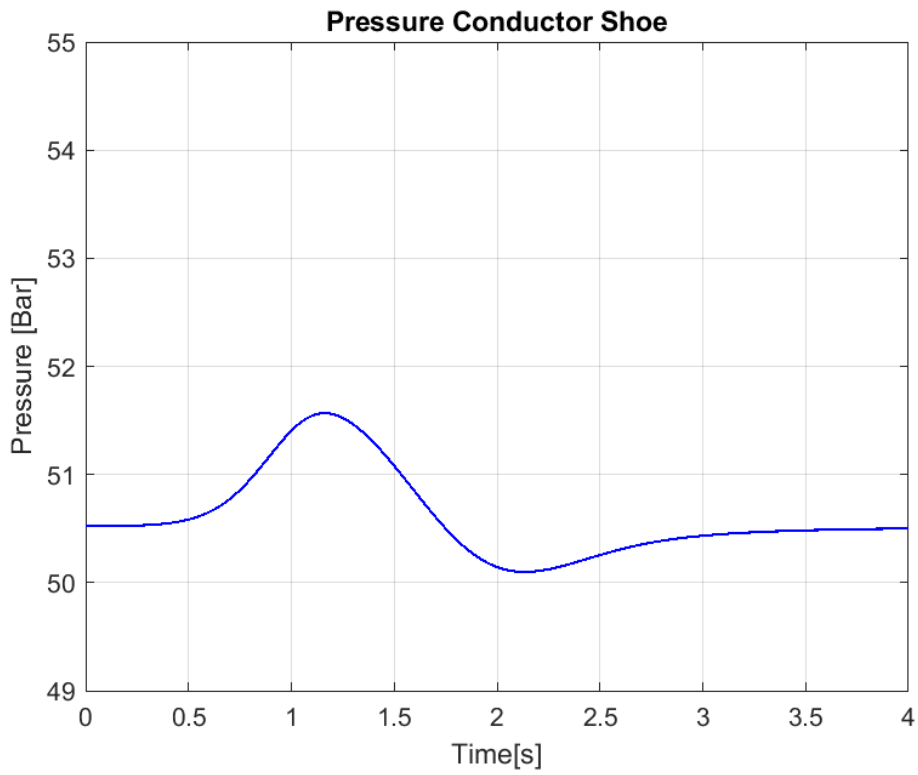

Figure 24: Pressure at the conductor shoe. Base case with sea water as drill fluid

Table 8: Wellbore pressure development for WBM #1

	Top Casing [bar]	Top Shoe Track [bar]	Bottom Hole [bar]	Conductor Shoe [bar]	Top Annulus [bar]
Initial	45,53	87,95	90,60	51,11	45,47
Pressure Max	114,47	155,20	101,42	52,21	45,79
Pressure Min	45,52	87,95	84,72	50,67	45,47
Pulse Magnitude	68,93	67,25	10,83	1,10	0,32
Pulse Dampening	0	1,68	58,11	67,83	68,61

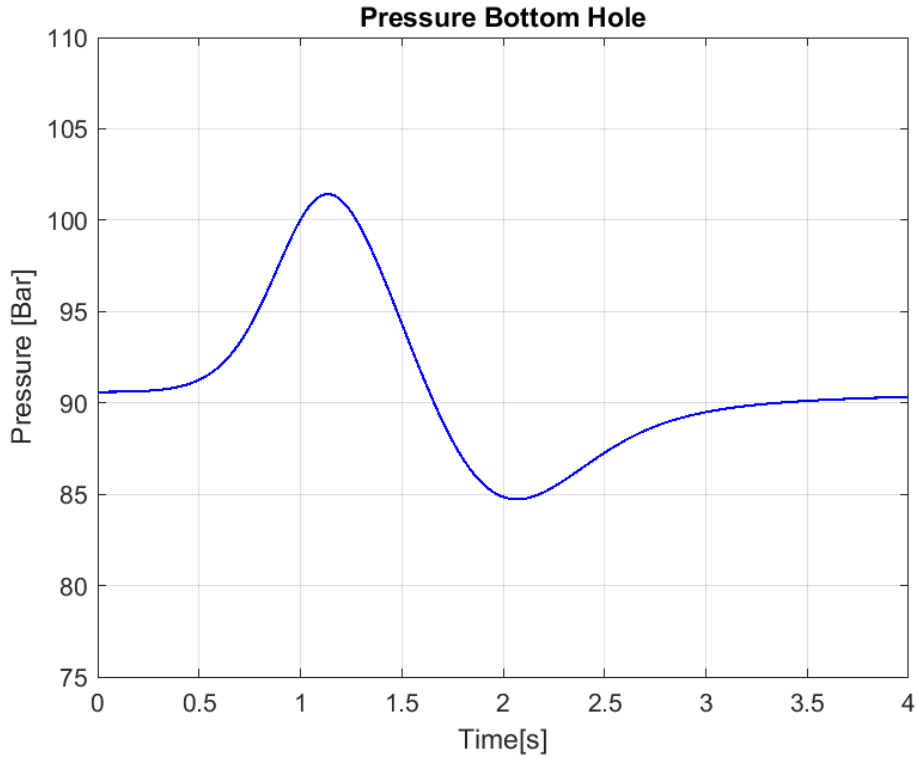

Figure 25: Pressure at bottom hole. Base case with WBM #1 as drill fluid

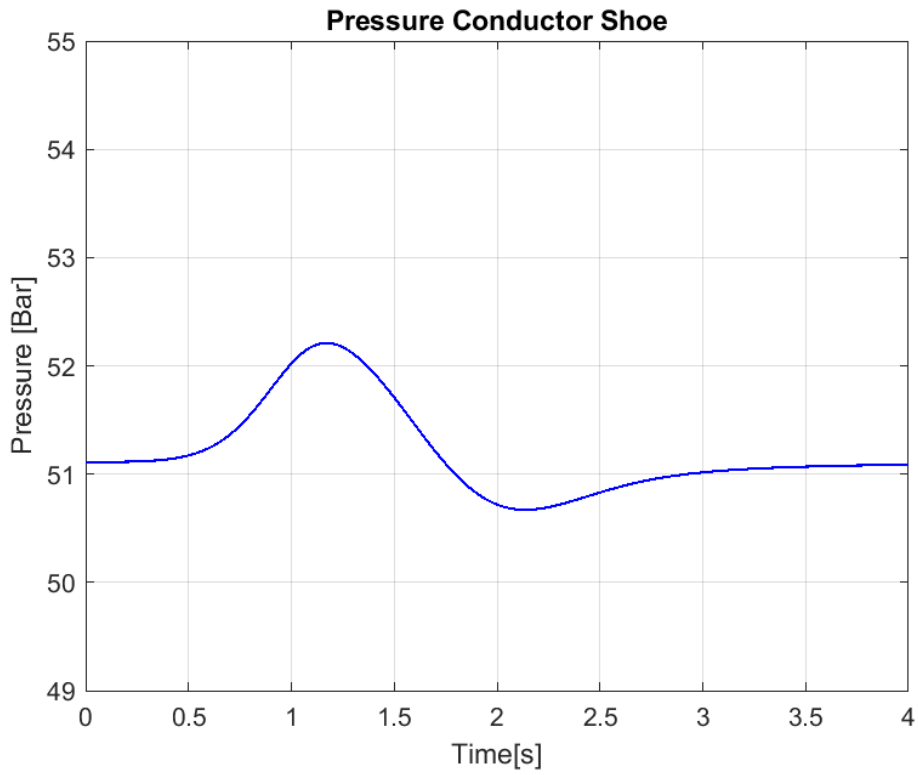

Figure 26: Pressure at the conductor shoe. Base case with WBM #1 as drill fluid

Table 9: Wellbore pressure development for WBM #2

	Top Casing [bar]	Top Shoe Track [bar]	Bottom Hole [bar]	Conductor Shoe [bar]	Top Annulus [bar]
Initial	45,53	91,64	94,52	51,60	45,47
Pressure Max	114,47	158,71	105,80	52,74	45,79
Pressure Min	45,52	91,64	88,46	51,14	45,47
Pulse Magnitude	68,94	67,07	11,28	1,14	0,32
Pulse Dampening	0	1,87	57,66	67,80	68,62

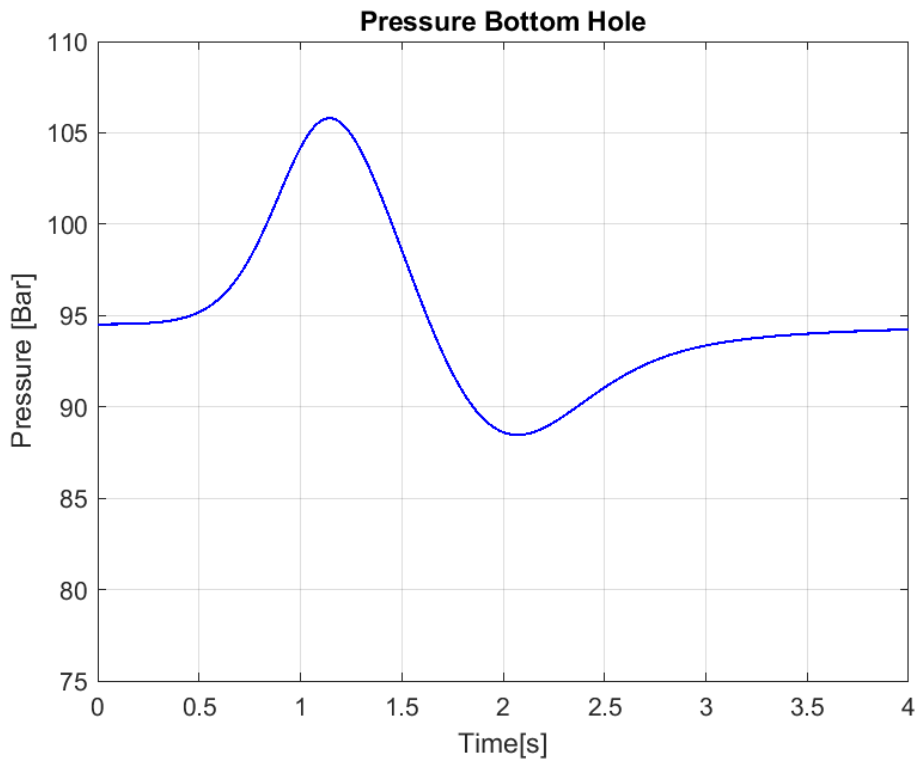

Figure 27: Pressure at bottom hole. Base case with WBM #2 as drill fluid

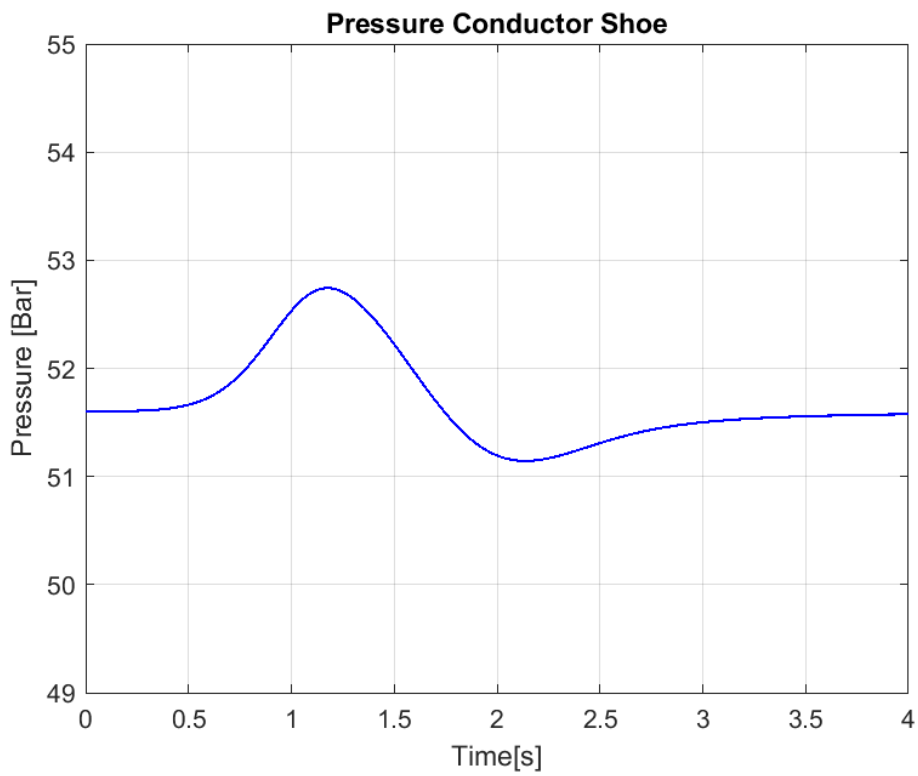

Figure 28: Pressure at the conductor shoe. Base case with WBM #2 as drill fluid

5.2 Dampening Effects

This section presents the results from altering system design parameters. Focus is directed to the parameters that are believed to consume the most energy and therefore represent the major dampening effects in the system. For this purpose, results from altering the diameter of flow restrictions, casing sizes, casing lengths and mud types are presented.

5.2.1 Extended Setting Depth

The maximum setting depth of the surface casing will in most cases be extended when using riserless mud recovery technology. The effects of increased casing lengths are presented in Table 10 through Table 13. The simulations were performed for surface casing setting depths of 600m BML and 700m BML. To investigate fluid effects, both WBM #1 and WBM #2 were simulated for each case. The simulated results are based on the same assumptions as for the base case, only with extended setting depths. Simulations with sea water as the drill fluid were not performed in this case, because it is assumed that higher mud weights from engineered muds are required in order to extend the setting depth of the surface casing.

The pressure loss due to frictional forces inside the surface casing, is described by the magnitude of pulse dampening at the top of the shoe track. From the bottom row in the tables below, it can be observed that this pressure loss increases with casing length. This is expected as the pressure pulse is exposed to a longer migration path and therefore more frictional forces from the casing walls. The pressure drop in the casing is estimated to be in between 4,09 - 4,47 bar for the casing length 600m and in between 5,70 - 6.10 bar for the casing length of 700m. It can also be observed that fluid type affects the results with 0,38 bar for a 600m casing string and with 0,40 bar for a 700m casing string. The trend of these results complies with the expected effect of increased frictional pressure loss for fluids with higher viscosity. The frictional pressure drop inside the casing is viewed as minor compared to the pressure drop across the shoe track.

According to the simulated results, the pressure drop across the shoe track will be in between 48,08 -49,01 bar for the 600m casing string and in between 44,29 - 45,28 bar for the 700m casing string. The trend is therefore decreasing pressure drop across the shoe track with increasing setting depth. As a subsequent result, the magnitude of the pressure wave at bottom hole will be higher at larger setting depths. This effect was unexpected, and it is further discussed in Chapter 6. The simulated results also indicate that the pressure pulse magnitude

at the conductor shoe is approximately 0,30 bar for both setting depths and both fluid types. This does not comply with the expected trend, as dissimilarities should have been induced by the difference in fluid viscosity.

Table 10: Wellbore pressure development - Setting depth 600m BML with WBM #1

	Top Casing [bar]	Top Shoe Track [bar]	Bottom Hole [bar]	Conductor Shoe [bar]	Top Annulus [bar]
Initial	45,53	110,51	113,16	51,11	45,47
Pressure Max	114,46	175,35	128,99	52,18	45,77
Pressure Min	45,52	110,51	105,19	50,74	45,47
Pulse Magnitude	68,92	64,83	15,83	1,07	0,30
Pulse Dampening	0	4,09	53,10	67,86	68,62

Table 11: Wellbore pressure development - Setting depth 600m BML with WBM #2

	Top Casing [bar]	Top Shoe Track [bar]	Bottom Hole [bar]	Conductor Shoe [bar]	Top Annulus [bar]
Initial	45,53	116,17	119,05	51,60	45,47
Pressure Max	114,46	180,62	135,43	52,70	45,77
Pressure Min	45,52	116,16	110,89	51,22	45,47
Pulse Magnitude	68,93	64,46	16,38	1,10	0,30
Pulse Dampening	0	4,47	52,55	67,83	68,63

Table 12: Wellbore pressure development - Setting depth 700m BML with WBM #1

	Top Casing [bar]	Top Shoe Track [bar]	Bottom Hole [bar]	Conductor Shoe [bar]	Top Annulus [bar]
Initial	45,53	121,80	124,44	51,11	45,47
Pressure Max	114,47	185,04	142,40	52,15	45,76
Pressure Min	45,52	121,80	115,67	50,77	45,47
Pulse Magnitude	68,94	63,24	17,95	1,04	0,30
Pulse Dampening	0	5,70	50,98	67,90	68,65

Table 13: Wellbore pressure development - Setting depth 700m BML with WBM #2

	Top Casing [bar]	Top Shoe Track [bar]	Bottom Hole [bar]	Conductor Shoe [bar]	Top Annulus [bar]
Initial	45,53	128,43	131,31	51,60	45,47
Pressure Max	114,46	191,26	149,84	52,66	45,76
Pressure Min	45,52	128,43	122,35	51,25	45,47
Pulse Magnitude	68,93	62,83	18,54	1,06	0,29
Pulse Dampening	0	6,10	50,39	67,87	68,64

5.2.2 Float Valve Diameter

The loss of energy across flow restriction is dependent on the diameter of the restriction. Narrower diameter normally results in a larger pressure drop. The effects from changing the valve sizes in the float collar and float shoe are presented in Table 14 and in Figure 29. Pressure drops presented in the table refers to the total pressure drop across the shoe track, which includes effects from the float collar, two casing joints and the float shoe. All the base case assumptions were applied for this simulation, except that the surface casing setting depth was set to 600m BML and WBM #1 was used as drill fluid.

Based on the results in prior sections, the effect of friction along the casing walls in the shoe track is assumed neglectable compared to the loss across the valves. The results in Table 14 are therefore believed to represent the pressure drop caused by the float valves respectively. The results show that the pressure drop decrease with increasing float diameter. This was an expected effect and it shows that the pressure pulse can be dampened by decreasing the size of the float valves. That being said, the valve size must also be large enough to handle the cement displacement rate. Therefore, the selection of valve size will be a trade-off between these two factors. As a reminder, the standard float valve size of 3,25 inches was used for the other simulations in this thesis.

Table 14: Valve diameter vs. pressure drop across shoe track

Diameter of Float Valves [in]	Pressure Drop Across Shoe Track [bar]
2.50	57,98
2.75	55,35
3.00	52,31
3.25	49,01
3.50	45,46

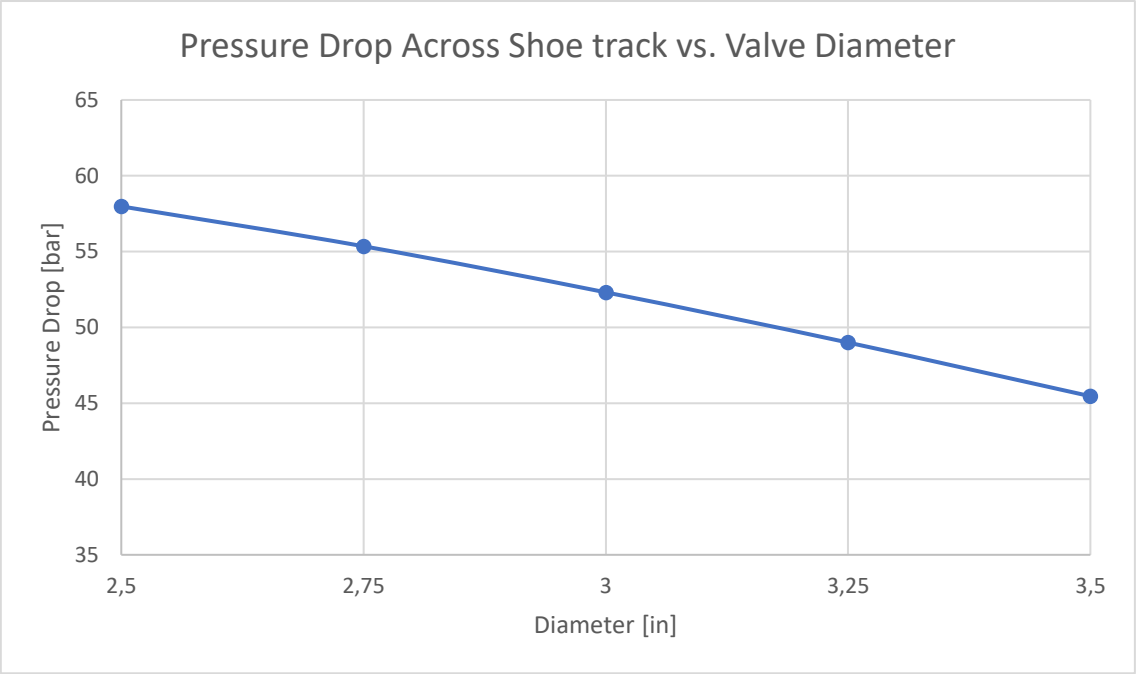

Figure 29: Pressure drop across the shoe track versus valve diameter

5.2.3 Effect of the Discharge Coefficients

As described in section 4.7.1 the pressure loss across valves is dependent on the discharge coefficient, which represents frictional effects across geometrical irregularities. The effect of altering the discharge coefficient for the float valves in the shoe track is presented in Table 15 and in Figure 30. The results were generated by simulations with all base case assumptions present, but with a surface casing setting depth of 600m BML and with WBM #1 as drill fluid.

The simulated results show that the pressure drop increases with decreasing discharge coefficient. Based on the results in prior sections, the effects from friction along the casing walls in the shoe track are assumed neglectable. The results in Table 15 are therefore believed to represent the pressure drop caused by the valve geometry respectively. The difference in pressure drop from the smallest coefficient to the largest is 8,86 bar, which indicates that considerable errors may be induced by wrong approximation of discharge coefficient.

Table 15: Discharge coefficient vs. pressure drop across shoe track

Discharge Coefficient of Float Valves [in]	Pressure Drop Across Shoe Track [bar]
0.4	53,43
0.45	51,25
0.50	49,01
0.55	46,76
0.60	44,57

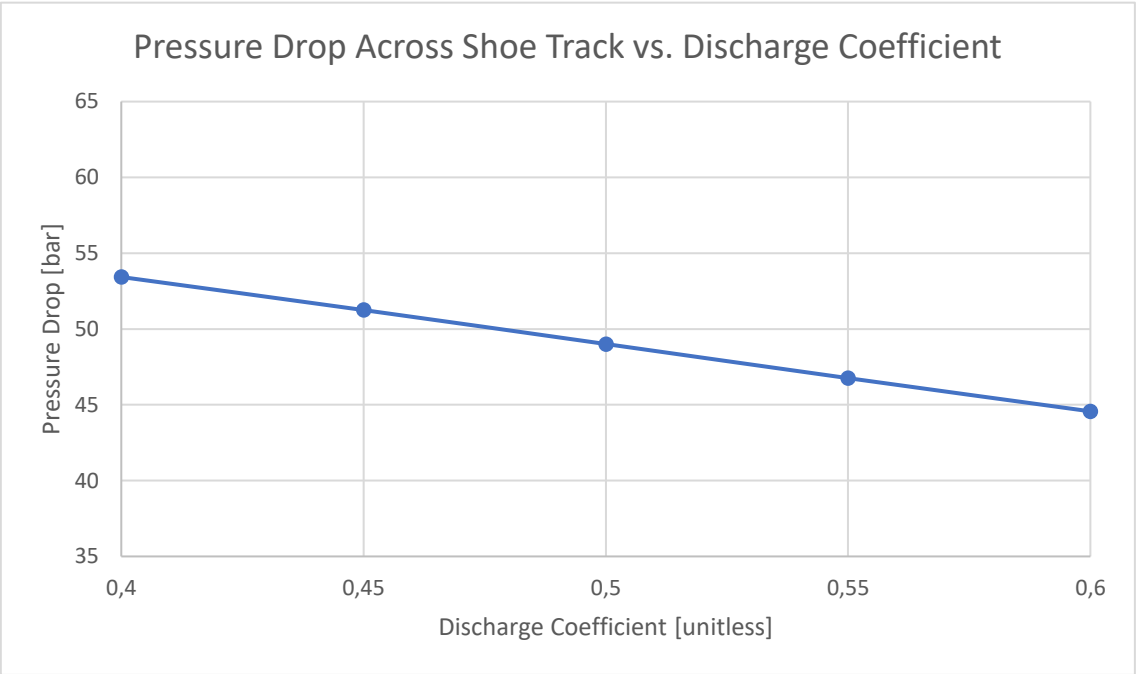

Figure 30: Pressure drop across shoe track vs. discharge coefficient

5.2.4 Casing Size

The simulated results for three generic casing sizes are presented below. The simulations were performed with all base case assumptions in place, but with a surface casing setting depth of 600m BML and with WBM #1 as drill fluid. The frictional pressure loss in the casing ($\Delta P_{f,IC}$), in the cased hole annulus ($\Delta P_{f,CA}$) and in the open hole annulus ($\Delta P_{f,OA}$) is presented in Table 16 and plotted in Figure 31. It can be observed that the frictional pressure loss increases with decreasing diameter of the fluid conduit. This trend was expected based on the equations in section 4.5.3, explaining the frictional pressure loss for non-Newtonian fluids. When the diameter is reduced, less flow area is available, and the fluid velocity will increase. According to equation 4.20 through 4.23, the increased velocity results in increased pressure loss and this corresponds with the trends in the simulated results.

It is important to understand that a change in casing size will affect the flow area of both the casing at the annulus, and therefore cause opposite effects for the pressure loss from the two conduits. This trend can be observed in Figure 31, where an increase in casing size reduces the pressure loss in the casing, but increase the pressure loss from the annulus. Based on the simulated result, the effect of changing the casing size is largest for a pressure drop across the cased hole annulus. This is the narrowest conduit, and the large effect is believed to be a product of the small flow area and great conduit length.

Table 16: Frictional pressure loss vs. casing size

OD [in]	ID [in]	$\Delta P_{f,IC}$	$\Delta P_{f,CA}$	$\Delta P_{f,OA}$
22	**20,75**	3,99	20,96	1,01
20	**18,73**	4,09	14,76	0,76
18,625	**17,775**	4,25	12,40	0,65

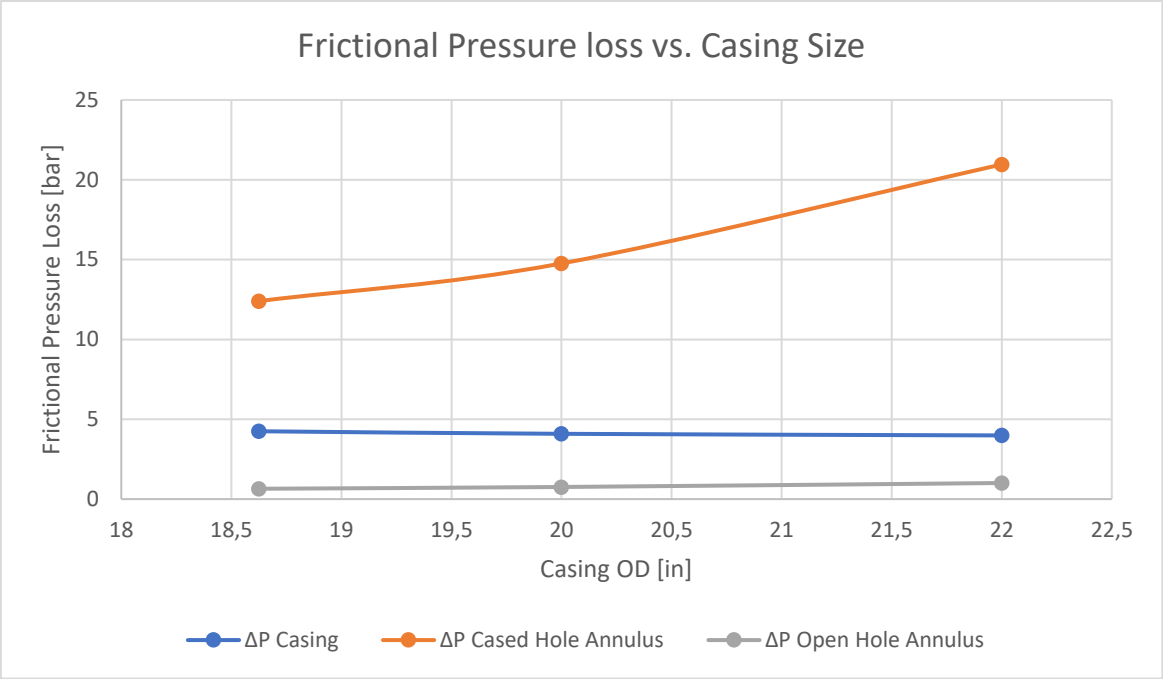

Figure 31: Frictional pressure loss vs. casing size

Table 17 presents the simulated magnitude of the pressure pulse for the different casing sizes. In the table P_{BH}, P_{CS} and P_{TA} denote the magnitude of the pressure pulse at bottom hole, at the conductor shoe and at the top of the annulus. The results state that an increased casing size provides a larger pulse magnitude at bottom hole. This trend could potentially be expected due to reduced frictional loss in the surface casing, but the variations pulse magnitude do not correspond to the with the frictional pressure losses in Table 16. It is therefore believed that some source of error affects these results. In addition, the questioned trend of exposing the conductor shoe to a pulse pressure of approximately 0,30 bar is also present for this simulation. The validity of these results and potential sources of error are further discussed in Chapter 6.

Table 17: Pulse magnitude at the bottom hole, conductor shoe and top annulus

OD [in]	ID [in]	P_{BH} [bar]	P_{CS} [bar]	P_{TA} [bar]
22	**20,75**	22.24	1.28	0,27
20	**18,73**	15,82	1,07	0,30
18,625	**17,775**	13.36	0,96	0,31

5.3 Enclosed System

The simulations presented in this section were performed with the purpose of investigating a worst case scenario. In the scenario, it is assumed that one valve on the MPC- system is connected to the pump, while the other one is closed. In addition, it is assumed that the pump cannot accept higher flow rate than it is already displacing, which value is set equal to the cement displacement rate. This implies that the system does not allow for fluid or pressure to escape the system. The results are presented in the Table 18 below. All the base case assumptions were applied, except that the surface casing setting depth was set to 600m BML and that WBM #1 was utilized as drill fluid.

Table 18: Wellbore pressure development for an enclosed top-hole system

	Top Casing [bar]	Top Shoe Track [bar]	Bottom Hole [bar]	Conductor Shoe [bar]	Top Annulus [bar]
Initial	45,53	110,51	113,22	51,17	45,53
Pressure Max	114,47	179,45	182,16	120,11	114,47
Pressure Min	45,52	110,51	113,21	51,17	45,52
Pulse Magnitude	68,94	68,94	68,94	68,94	68,94
Pulse Dampening	0	0	0	0	0

It can be observed that since no flow or pressure is allowed to escape the system, all energy is retained within the system. This situation can be compared to applying force to a piston in an enclosed cylinder, which results in a pressure increase as long as the force is applied to the piston. The pressure magnitude of the results is probably not representable because, either the formation or the MPC valves are likely to break before reaching this pressure level.

6 Discussion

The scope of this thesis was to investigate pressure pulses from releasing the wiper plug for cement displacement. Since there were little literature and research available on this topic, the theoretical fundament and digital model were basically built from scratch. In such a design process, there will always be uncertainty related to the assumptions and to the digital representation of the physical phenomenon. This chapter will discuss the validity of the simulated results, aspects with the model and sources of error.

6.1 Applicability of Using Simscape Fluids as Simulation Software

The applicability of using Simscape Fluids for simulating pressure transients in a top-hole system, has been evaluated based on two criteria.

The first criterion is the usefulness for constructing a digital representation of the physical system. For this purpose, the software stands out as good for practical approaches, but with drawbacks for high accuracy purposes. This statement is based on limitations in the pre-made component library, which result in some rough approximations for the digital representation of the system. For instance, some major components like fluid conduits can be modeled directly from the block library and provides adequate representations. On the other end, components like the spring actuated float valves in the shoe track are not available and must be approximated by generic flow restriction blocks. That being said, the generic blocks have many options for altering the component properties and can potentially become good approximations if properly adjusted. On the other hand, this would require access to detailed information on pressure losses across the physical valve.

The second criterion is the capacity of performing precise simulations of cementing operations with dynamic pressure. Unfortunately, the software turns out to be poorly fitted for this purpose due to several reasons. First, the software is limited to simulating only one fluid type in the system. This decreases the flexibility for simulating cement operations, since several fluids like displacement fluid, cement slurry and spacer fluid are present. Secondly, the Simscape software is not designed for simulating non-Newtonian fluids. Therefore, a large amount of work was required to design and implement non-Newtonian rheology models, used for calculating frictional pressure losses in the fluid conduits. Thirdly, the boundary conditions available for fluid systems turned out to be insufficient for simulating transient pressure events of this type. This affects the simulated results and will be further discussed in

section 6.2 below. As a result, it has turned out that Simscape Fluid is not an optimal software for the purpose of this thesis. Evaluation of alternative simulation software's should therefore be assessed for the purpose.

6.2 Validity of Simulated Results

It is challenging to evaluate the validity of the simulated results due to several reasons. For instance, there exist little research and literature on this specific phenomenon. As a result, no basis of comparison has been available, and the validity of the results has therefore been evaluated based on other aspects. The sections below discuss the validity of the results based on the fundamental theory, assumptions, and the digital approximations.

In view of the author, there are two main sources of uncertainty in the simulations. The first one is related to the characteristics of the block named Reservoir (TL), described in Appendix G: Block Descriptions. This block models the boundary conditions for the fluid system and contains a constant reservoir pressure. During model construction this block was believed to provide adequate boundary conditions, but the simulated results have indicated unexpected trends. Later investigation confirms that this block alters the pressure of fluids moving in and out of the reservoir, to be equal to the constant reservoir pressure. This error explains the questionable trend in the simulated results, where a pressure pulse magnitude of approximately 0,3 bar was measured at the top of the annulus for all simulations. The measured magnitude reflects the last pressure drop to equalize pressure across the valve to the reservoir.

The error in the boundary condition is further believed to affect the pressure pulse development in other parts of the well, as the model aims for zero transient pressure at the reservoir inlet. This is also supported by the trends in Table 16 and Table 17, where the difference in bottom hole pressure corresponds to the changes in annular pressure loss for the different casing strings. As a consequence, the validity of the simulated pressure pulse magnitudes is questionable and likely to be non-realistic. The level of confidence to the simulated results is therefore strongly reduced. Unfortunately, no better option was found in the Simscape block library for implementing a better set of fluid system boundary conditions. Alternative measures for solving this problem are discussed in 6.4.

The second main source of uncertainty is related to representation of the spring actuated float valves in the float collar and the float shoe. As can be seen from results in Chapter 5, the pressure drop across these valves is significant and the magnitude is affected by the valve geometry. A poor digital representation of these valves can result in large deviations from the real pressure loss and therefore reduce the level of confidence for the simulated results. This uncertainty can probably be reduced with access to data describing measured pressure drops across the physical valves at several flow conditions. Unfortunately, this kind of information has not been available, and a basis of comparison could not be developed.

Another factor that affects the validity of the result, is the period and amplitude of the approximated pressure signal from the signal generator. It was assumed that pressure amplitude of the generated signal was equal to the shear pin strength. This implies that all energy is transmitted into the fluid as pressure during the release process. The assumption probably overestimates the amplitude of the pressure pulse because some energy will be lost to the surroundings during the plug release process. The question of how much energy that is lost during the release process needs further investigation.

The period of the initial pressure signal reflects the time it takes for the pressure to equalize across the wiper plug, after breaking the shear pins. This period of time will depend on the rate at which the compressed fluid in the landing string is allowed to expand. To estimate this time period, an analysis of plug acceleration must probably be performed and compared to the rate at which the landing string volume expands. This analysis is complex, and the initial signal was therefore assumed to have a period of approximately two seconds as illustrated in Figure 22. This time period allowed for smooth simulations, which was the main argument for the basic approach in this thesis. It can be discussed if this period of time is too long, resulting in unrealistically long exposure time for the formation. On the other hand, pressure induced damages to formation and equipment are assumed to take place instantaneously for basic approaches and therefore to be dependent on the pressure amplitude only.

On the positive end, the digital model provides reasonable trends for pressure losses at some points. For instance, the results from Table 14 state that pressure drop increases with decreasing nozzle size. This is both reasonable and expected, because the reduced flow area provides higher fluid velocity and therefore more turbulence. It is also likely that the valves will constitute a major portion of the pressure loss in the physical system. This is based on the general trend in the simulations, where the loss across the vales on average constituted 82% of the total loss for the base cases and 68% for the cases with extended setting depth.

6.3 Effects on Formation and Equipment

The downhole formation will be exposed to an additional pressure equal to the magnitude of the pressure pulse. From the simulated results in Chapter 5, the magnitude of the pressure pulse was estimated to be in between 10,21 – 11,28 bar for a setting depth of 400m BML. The same magnitude was estimated to 15,83 – 16,38 bar and 17,95-18,54 bar for setting depths of 600m BML and 700m BML, respectively. The discussion below assumes that these results are valid.

In order to evaluate if these pressure magnitudes are sufficient to damage the formation, the results should be compared to the formation fracture gradient at the respective well location. On the other hand, it is believed that the simulated pulse magnitudes are strong enough to cause damage to the formation in several cases. Especially for cases with narrow drilling windows, where the presence of RMR-technology is already required to balance the wellbore pressure. In general, the formation strength increases with depth and a stronger formation can therefore be expected for the simulations with extended setting depth. On the other hand, the magnitude of the pressure pulse was estimated to increase for these setting depths and therefore increase the risk of damaging the formation. Further investigation is therefore required to evaluate if the pulse magnitude can break the formation.

Based on the simulated results from Chapter 5, the pressure pulse is not believed to cause damage to the valves on the MPC- system due to low magnitudes. The only exemption is the simulated case for an enclosed system, where the formation or the MPC-valve was expected to break, depending on which one that states the weakest point.

It can also be discussed if the conductor shoe states a weak point in the top-hole system. This will be dependent of the formation strength at the well locations and the setting depth of the conductor. When considering the results from the calculations of conductor lengths in Table 3, it can be observed that the installation method affects the length of the conductor. It can therefore be discussed if the CAN- design provides a weaker shoe than the alternatives, but again this is heavily dependent on the formation properties at the location.

6.4 Recommendations for Future Work

The most important improvement at the current stage, is to increase the level of confidence for the simulated results. Most of this uncertainty is related to the effect of fluid boundary conditions and to the digital representation of the float valves. It is therefore recommended to pursue an improved design for these parts of the model, with the boundary conditions as highest priority. For this purpose, it is recommended to investigate opportunities of building blocks from scratch and see if these can provide adequate boundary conditions for the fluid system. In case this turns out to be difficult, the contingency of using an alternative software is recommended. A potential candidate that should be evaluated for this purpose is LVTrans, which is an open source software used for transient simulations in piping systems (Svingen 2020). The software is made in LabView, which can be accessed through the NTNU software library.

Several options are available for improving the representation of the float valves. For instance, float valve vendors can be contacted, with inquiries for component data that provides information on frictional effects or pressure losses across the valves. By accessing such information, the block properties could be adjusted to more representative values. The Simscape software also has capacity for creating user defined blocks with specific properties. This alternative should also be further investigated for accurate valve representation.

Another recommended measure for improving the level of confidence, is to collect relevant operational data from operators on the NCS and use these as a basis of comparison for the simulated results. This could include historical pressure plots from top hole cementing operations, drilling reports or operational experience with the pressure pulse phenomenon. Also, it is believed that pressure data from the suction module on the RMR- system could provide valuable information on transient pressure events in the well.

Experimental activities are recommended in order to increase the knowledge on propagating pressure pulses in top-hole system, but also for accessing data which can be used for comparison to the simulations. It would for instance be interesting to investigate the pressure drop across spring actuated float valves, which is probably possible in laboratory designed for high pressure experiments. Another possibility is construction of a down-scaled top hole system in the wellbore at the laboratory of the Department of Geoscience and Petroleum at NTNU. Further assessment must be carried out in order to evaluate the potential outcome versus the economic costs of such experiments.

7 Conclusion

The values presented in the following conclusion are based on the assumptions and approximations described in section 4.7 and throughout the rest of Chapter 4. Some important assumptions are the presence of only one fluid type in the system, float valves approximated as flow restrictions and perfect reflection of the pressure pulse at bottom hole. The validity and effects of these assumptions were discussed in Chapter 6.

- The simulations show that a pressure pulse is created by breaking the shear pins and releasing the wiper plug. It is also shown that the pulse is exposed to dampening effects in terms of energy losses, while it propagates through the top-hole system.
- The base case simulations show that the downhole formation will be exposed to an additional pressure of 10,21 - 11,28 bar from the pressure pulse, depending on the fluid type. Trends from extending the surface casing setting depths showed an increase in pulse magnitude at bottom hole, with the highest value of 18,54 bar for a setting depth of 700m BML. Based on these results, it is believed the pressure pulse can damage the downhole formation in cases where narrow drilling windows are present.
- The simulations indicate that a large portion of the pulse energy is lost across the float valves in the shoe track. This portion was on average estimated to constitute 82% of the total pressure loss in the base case simulations. The same energy loss was simulated to be 70,7% and 65,2% on average for setting depths of 600m BML and 700m BML, respectively.
- The frictional pressure loss for a migrating pulse was proven to be affected by the flow area and the length of fluid conduits. Simulations show that the highest frictional pressure drop takes place across the cased hole annulus. For this conduit, the average pressure loss was estimated to be 9,7 bar for a setting depth of 400m BML, 15,0 bar for a setting depth of 600m BML and 17,2 bar for a setting depth of 700m BML.
- Pressure loss across the float valves correlate with the expected trend of increased pressure loss for decreased float valve diameter. A simulated case showed that a change from 2,5 inches to 3,5 inches in valve diameter, resulted in a pressure loss reduction of 12,52 bar.
- Sources of error are related to the boundary conditions for the fluid system and to the representation of float valves. Recommendations for future work are therefore to evaluate alternative simulation software's and to develop more knowledge on the phenomenon, in order to reduce the degree of uncertainty for the simulated results.

Nomenclature

BOP	Blow Out Preventer
BML	Below Mud Line
CC	Power and Control Container
DGD	Dual Gradient Drilling
ECD	Equivalent Circulating Density
ID	Inner Diameter
LPWHH	Low Pressure Wellhead Housing
MPC	Manage Pressure Cementing
MRL	Mud Return Line
NCS	Norwegian Continental Shelf
NTNU	Norwegian University of Science and Technology
OBM	Oil Based Mud
OD	Outer Diameter
OTC	Office and Tool Container
RKB	Rotary Kelly Bushing
RMR	Riserless Mud Recovery
ROV	Remotely Operated Vehicle
SMO	Suction Module
SPM	Suction Pump Module
TL	Thermal Liquid
TVD	True Vertical Depth
UW	Umbilical and Umbilical Winch
WBM	Water Based Mud

Q	Axial load capacity [KN]
RF	Reduction factor [unitless]
cs	Undrained soil shear strength [KPa]
z	Depth [m]
c	Speed of sound in fluid [m/s]
f	Frequency [s^{-1}]
L	Length [m]
N	Number of pipe segments [unitless]
$\dot{m}$	Mass flow rate [kg/s]
$\ddot{m}$	Mass flow rate derivative [kg/s^2]
V	Internal pipe volume [m^3]
ρ	Density [kg/m^3]
β	Bulk modulus [GPa]
α	Thermal expansion coefficient [k^{-1}]
T	Temperature [k]
$\dot{T}$	Rate of temperature change [k/s]
P	Pressure [Pa]
$\dot{p}$	Rate of pressure change [Pa/s]
g	Gravity constant [m/s^2]
S	Cross sectional flow area [m^2]
ϕ	Energy flow rate [J/s]
$\dot{E}$	Energy accumulation rate [J/s]
u	Internal energy [J/kg]
t	Time [s]
Re	Reynolds number [unitless]
D_h	Hydraulic diameter [m]
A_c	Cross sectional pipe area [m^2]
p	Wetted perimeter [m]
f_D	Darcy friction factor [unitless]
λ	Pipe shape factor [unitless]
ϵ	Absolute pipe roughness [mm]
τ	Shear stress [Pa]
τ_γ	Yield shear stress (yield point) [Pa]
μ	Viscosity [Pa s]
μ_p	Plastic viscosity [Pa s]
μ_a	Apparent viscosity [Pa s]
$\dot{\gamma}$	Shear rate [s^{-1}]
d	Diameter [m]
$\bar{v}$	Average fluid velocity [m/s]
q	Volumetric flow rate [m^3/s]
ΔP	Pressure drop [Pa]
C_d	Discharge coefficient [unitless]
Δ	Delta operator [unitless]
π	Pi constant [unitless]
e	Euler's constant [unitless]
#	Type number for drill fluid

References

Aird, Peter. 2018. *Deepwater Drilling*, 1. Edition edition, 295. elsevier.com: Gulf Professional Publishing.

Aleksandersen, Jostein and Higgins, Colin. 2019. *Neodrill Saves Costs for Siccar Point at Cambo*. oedigital.com: Offshore Engineer. https://www.oedigital.com/news/471400-neodrill-saves-costs-for-siccar-point-at-cambo.

Brechan, Bjørn A., Corina, Anisa N., Gjersvik, Tor B. et al. 2017. Compendium TPG 4215 Drilling Engineering **Revision 1** (NTNU - Department of Petroleum Engineering and Applied Geophysics): 340-383, 584-618.

Bøe, Arnt Even. 2011. *Glemmer aldri brølet fra gassen*. aftenbladet.no: Stavanger Aftenblad. https://www.aftenbladet.no/aenergi/i/LPr5x/ndash-glemmer-aldri-brlet-fra-gassen.

Cengel, Yanus A. and Cimbala, John M. 2014. *Fluid Mechanics: Fundamentals and Applications* Third Edition in SI Units edition, 350, 392-394. United States of America: McGraw-Hill Education.

Claudey, Eric, Maubach, Caroline, and Ferrari, Sandy. 2016. Deepest Deployment Of Riserless Dual Gradient Mud Recovery System In Drilling Operation In The North Sea. Presented at the SPE Bergen One Day Seminar, Grieghallen, Bergen, Norway. 2016/4/20/. https://doi.org/10.2118/179999-MS.

Elahifar, Behzad. 2020. *Written and verbal communication with co-supervisor*.

Enhanced Drilling. 2019. *Riserless Mud Recovery System Brochure* enhanced-drilling.com, Enhanced Drilling. https://www.enhanced-drilling.com/bilder/brochure_RMR/files/assets/common/downloads/publication.pdf.

Enhanced Drilling. RMR-Riserless Mud Recovery *Enhanced Drilling*, https://www.enhanced-drilling.com/solutions/rmr-riserless-mud-recovery (accessed 15.04.2020.

Guo, Boyun and Liu, Gefei. 2011. *Applied Drilling Circulation Systems*, 1st Edition edition, 19-42. elsevier.com: Gulf Professional Publishing.

IADC. 2020. *Drilling margin/window*. drillingmatters.iadc.org, International Association of Drilling Contractors. https://drillingmatters.iadc.org/glossary/drilling-marginwindow/.

Integrated Ocean Drilling Program (IODP). 2010. *CHIKYU to Set Sail for Expedition 332 NanTroSEIZE Stage 2: Riserless Observatory-2*. jamstec.go.jp/e/, Japan Agency for Marine-Earth Science and Technology. https://www.jamstec.go.jp/e/about/press_release/20101022/.

Mathis, Wolfgang, Strand, Harald, and Hollinger, Gerald. 2017. Case History: How to Enable the Horizontal Development of Shallow Reservoirs. Presented at the SPE/IADC Drilling Conference and Exhibition, The Hague, The Netherlands. 2017/3/14/. https://doi.org/10.2118/184667-MS.

Miljødirektoratet. DEA Norge søker om boring av Toutatis. *Miljødirektoratet* 29.04.2019, https://tema.miljodirektoratet.no/no/Horinger/Petroleum/DEA-Norge-AS-soker-om-boring-av-Toutatis-20195592/ (accessed 15.04.2020.

Neodrill AS. Neodrill Track Record https://www.neodrill.com/track-record (accessed 13.03.2020.

Ormestad, Helmut. 2018. *bølge*. snl.no, Store norske leksikon. https://snl.no/b%C3%B8lge.

Prasertamporn, Praisont. 2016. Enhanced Deepwater Conductor Jetting Design for East Malaysia. Presented at the International Petroleum Technology Conference, Bangkok, Thailand. 2016/11/12/. https://doi.org/10.2523/IPTC-18738-MS.

Reksterberg, Kristine and Kvassheim, Marie. 2011. *Deepwater Riserless Drilling*. Master, Norwegian University of Science and Technology Trondheim (20 May 2011).

Skalle, Pål. 2015. *Pressure Control During Oil Well Drilling* 6th edition edition. bookboon.com.

Smith-Solbakken, Marie and Vinnem, Jan Erik. 2020. *West Vanguard-Ulykken*. snl.no: Store Norske Leksikon. https://snl.no/West_Vanguard-ulykken.

Smith, Dave, Tarr, Brian, Winters, Warren J. et al. 2010. Deepwater Riserless Mud Return System for Dual Gradient Tophole Drilling. Presented at the SPE/IADC Managed Pressure Drilling and Underbalanced Operations Conference and Exhibition, Kuala Lumpur, Malaysia. 2010/1/1/. https://doi.org/10.2118/130308-MS.

Standards Norway. 2004. *NORSOK Standard D-010* Annex A Table A.1: Well Inetgrity in Drilling and Well Operations Standards Norway. https://www.standard.no/pagefiles/1315/d-010r3.pdf.

Stave, Roger, Fossli, Børre, Endresen, Cato et al. 2014. Exploration Drilling with Riserless Dual Gradient Technology in Arctic Waters. Presented at the OTC Arctic Technology Conference, Houston, Texas. 2014/2/13/. https://doi.org/10.4043/24588-MS.

Stave, Roger, Nordas, Philip, Fossli, Borre et al. 2014. Safe and Efficient Tophole Drilling using Riserless Mud Recovery and Managed Pressure Cementing. Presented at the Offshore Technology Conference-Asia, Kuala Lumpur, Malaysia. 2014/3/25/. https://doi.org/10.4043/25462-MS.

Svingen, Bjørnar. LVTrans Open source transient simulations software for hydraulic piping systems. *Svingen Tech*, http://svingentech.no/index.html (accessed 01.06.2020.

The MathWorks Inc. 2020a. *Simscape™ Fluids™ Reference*. mathworks.com: Matlab&Simulink, The MathWorks Inc. https://se.mathworks.com/help/pdf_doc/physmod/hydro/hydro_ref.pdf.

The MathWorks Inc. 2020b. *Simscape™ Fluids™ Users's Guide*. mathworks.com: Matlab&Simulink The MathWorks inc. https://se.mathworks.com/help/pdf_doc/physmod/hydro/hydro_ug.pdf.

Thorogood, John Laurence, Rolland, Nils Lennart, Brown, John D. et al. 2007. Deployment of a Riserless Mud Recovery System Offshore Sakhalin Island. Presented at the SPE/IADC Drilling Conference, Amsterdam, The Netherlands. 2007/1/1/. https://doi.org/10.2118/105212-MS.

Van Noort, Roger, Murray, Rob, Wise, James et al. 2009. Conductor Pre-Installation, Deepwater Brazil. Presented at the Offshore Technology Conference, Houston, Texas. 2009/1/1/. https://doi.org/10.4043/20005-MS.

Weatherford International. 2005. *Float & Stage Equipment*, 44. weatherford.com, Weatherford. https://www.weatherford.com/en/documents/catalog/float-and-stage-equipment/.

Weatherford International. 2013. *Casing Wiper Plugs and Darts*, 58. weatherford.com, Weatherford. https://www.weatherford.com/en/documents/catalog/casing-wiper-plugs-and-darts/.

Weatherford International. 2016. *Casing Accessories*, 54. weatherford.com, Weatherford. https://www.weatherford.com/en/documents/catalog/casing-accessories/.

Appendix A: Well Trajectory for Shallow Reservoir Layer

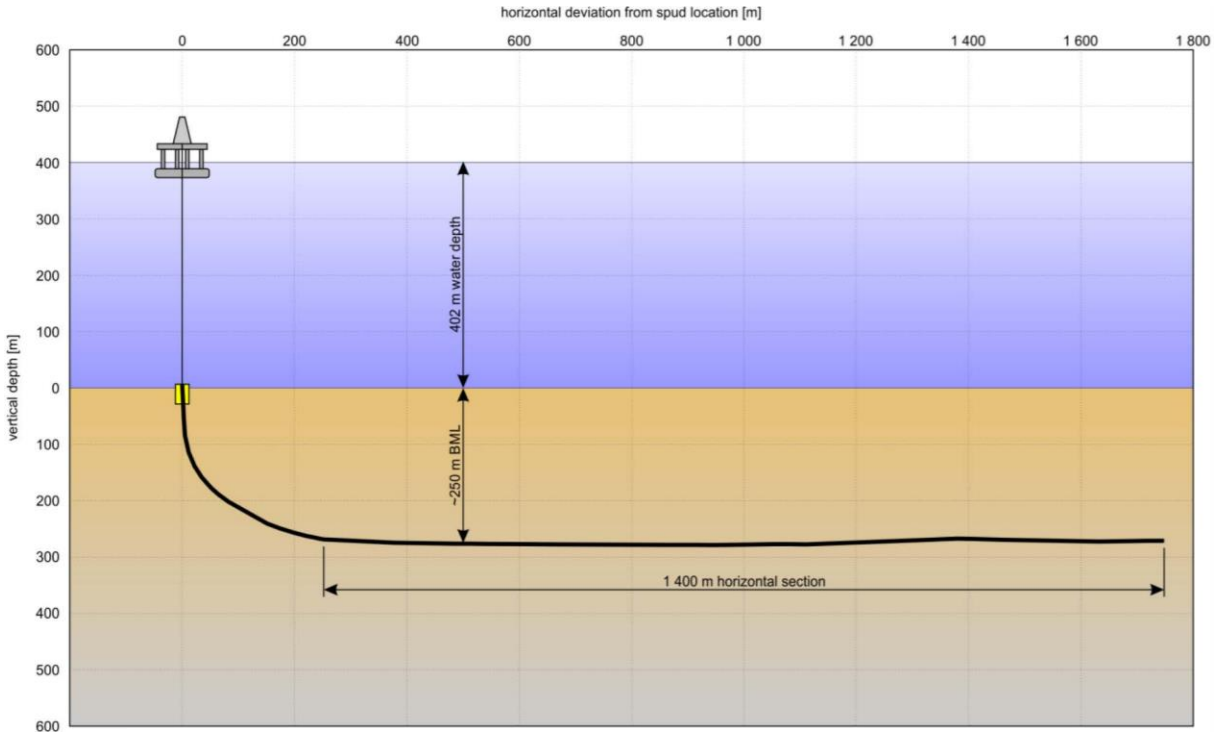

Figure 32: Well trajectory with shallow kick off point (Mathis et al. 2017)

Appendix B: Calculation of Jetted Conductor Lengths

This is a ruff calculation for estimating the required length of a jetted conductor, to provide the same axial load capacity as the two CAN-design in Table 2. Equation B.1 is provided by Aird (2018) and it is utilized to find the required conductor length

$$Q = RF * \pi * d_o * \int_{z_1}^{z_2} cs\, dz \tag{B.1}$$

Q	= Axial load capacity [KN]	Z_1	= Depth BML top conductor [m]
RF	= Reduction factor [N/A]	Z_2	= Depth BML shoe conductor [m]
d_o	= Outer Diameter [m]	cs	= Undrained soil shear strength [KPa]
		z	= Depth BML [m]

Undrained soil shear strength cs is approximated as a linear function for this calculation, where the shear strength is proportional to the depth BML. The linear function is provided in Eq. B.2, where a and b are constants.

$$cs = az + b \tag{B.2}$$

By integration of the shear strength cs along the conductor from Z_1 to Z_2, Eq. B.3 is obtained.

$$\int_{z_1}^{z_2} cs\, dz = [\frac{a}{2} \cdot z^2 + b \cdot z]_{z_1}^{z_2} \tag{B.3}$$

It is assumed that the conductor fully penetrated the seabed during installation, so Z_1 = 0m BML. By inserting Z_1=0 into Eq. B.3, it is reduced to Eq. B.4:

$$\int_{L_1}^{L_2} cs\, dz = \left(\frac{a}{2} \cdot {Z_2}^2 + b \cdot Z_2\right) \tag{B.4}$$

Then, by inserting Eq. B.4 into Eq. B.1 and rearrange all terms to the left hand side, Eq. B.5 is obtained.

$$\left(\frac{RF \cdot \pi \cdot d_o \cdot a}{2}\right) \cdot {Z_2}^2 + (RF \cdot \pi \cdot d_o \cdot b) \cdot Z_2 - Q = 0 \tag{B.5}$$

Eq. B.5 is a quadratic equation. Z_2 is therefore found by solving Eq. B.5 with the quadratic formula in Eq B.6, often referred to as the ABC-formula. This calculation will provide a negative and a positive solution, but only the positive solution is physical valid.

$$Z_2 = \frac{-B \pm \sqrt{B^2 - 4 \cdot A \cdot C}}{2 \cdot A} \tag{B.6}$$

The input variables for the quadratic formula is given below. Variables a and b in Eq. B.2 are calculated based on the soil data in Table 1. There is one C-term for each CAN design, C_{short} for the short CAN and C_{Long} for the long CAN. Input values and results are provided in Table 19.

$$a = \frac{(CS_2 - CS_1)}{(Z_2 - Z_1)} \qquad b = CS_1 \qquad A = \left(\frac{RF \cdot \pi \cdot d_o \cdot a}{2}\right) \qquad B = (RF \cdot \pi \cdot d_o \cdot b)$$

$$C_{Short} = Q_{Short} \qquad C_{Long} = Q_{Long}$$

The calculations are performed with the assumptions that the outer diameter of the conductor is 30 inch and that the conductor fully penetrated the seabed during installation. The reduction factor RF is dependent on the soil disturbance during installation (Aird 2018). RF is assumed to be 0,8 for this calculation, meaning that the soil has regained 80% of the original undrained shear strength. This implies that some time have been spent after installation, to let the conductor soak into place.

Table 19: Input data and results for jetted conductor lengths

Type	Value	Unit
RF	0,8	[unitless]
OD	0,762	[m]
$\mathbf{Z_1}$	0	[m]
a	3,11	[KPa/m]
b	6	[KPa]
$\mathbf{Q_{Short}}$	3606	[KN]
$\mathbf{Q_{Long}}$	7010	[KN]
A	2,978	[KN/m^2]
B	11,491	[KN/m]
$\mathbf{C_{Short}}$	3606	[KN]
$\mathbf{C_{Long}}$	7010	[KN]
$\mathbf{Z_{2_Short}}$	32,92	[m]
$\mathbf{Z_{2_Long}}$	46,63	[m]

The results of this ruff calculation shows that a jetted conductor length of 32,92m is required to provide the same axial load capacity as the short CAN-design in Table 2. It also shows that a jetted conductor length of 46,63m is required to provide the same axial load capacity as the long CAN-design in Table 2.

Appendix C: Acceptance Criteria for Casing Float Valves

15.41 Table 41 – Casing float valves

Features	Acceptance criteria	See
A. Description	The element consists of a tubular body and an internal one-way valve.	
B. Function	The purpose is to prevent flow of fluids from the wellbore up the casing/liner during installation of casing/liner and to allow for circulating the well.	
C. Design construction selection	1. The element shall allow for pumping fluids down the casing/liner but prevent any flow in the opposite direction. 2. The element shall withstand expected burst, collapse and axial loads including design factors. 3. The working/sealing pressure of the element shall be equal to the maximum differential pressure across the element plus a defined safety factor. 4. The element shall function at expected wellbore conditions with regards to differential pressure, temperature and fluid characteristics. 5. There shall be a minimum of two casing float valves. A convertible casing float (autofill) can be used when there are no sources of inflow exposed.	ISO 10427-3
D. Initial test and verification	1. Specifications and performance shall be documented by vendor. 2. Should be inflow/function tested during casing/liner running.	
E. Use	Shall be installed according to vendor's procedure.	
F. Monitoring	Not applicable after initial testing	
G. Common well barrier	None	

Figure 33: Acceptance criteria for casing float valves (Standards Norway 2004)

Appendix D: Steps in Conventional Cementing

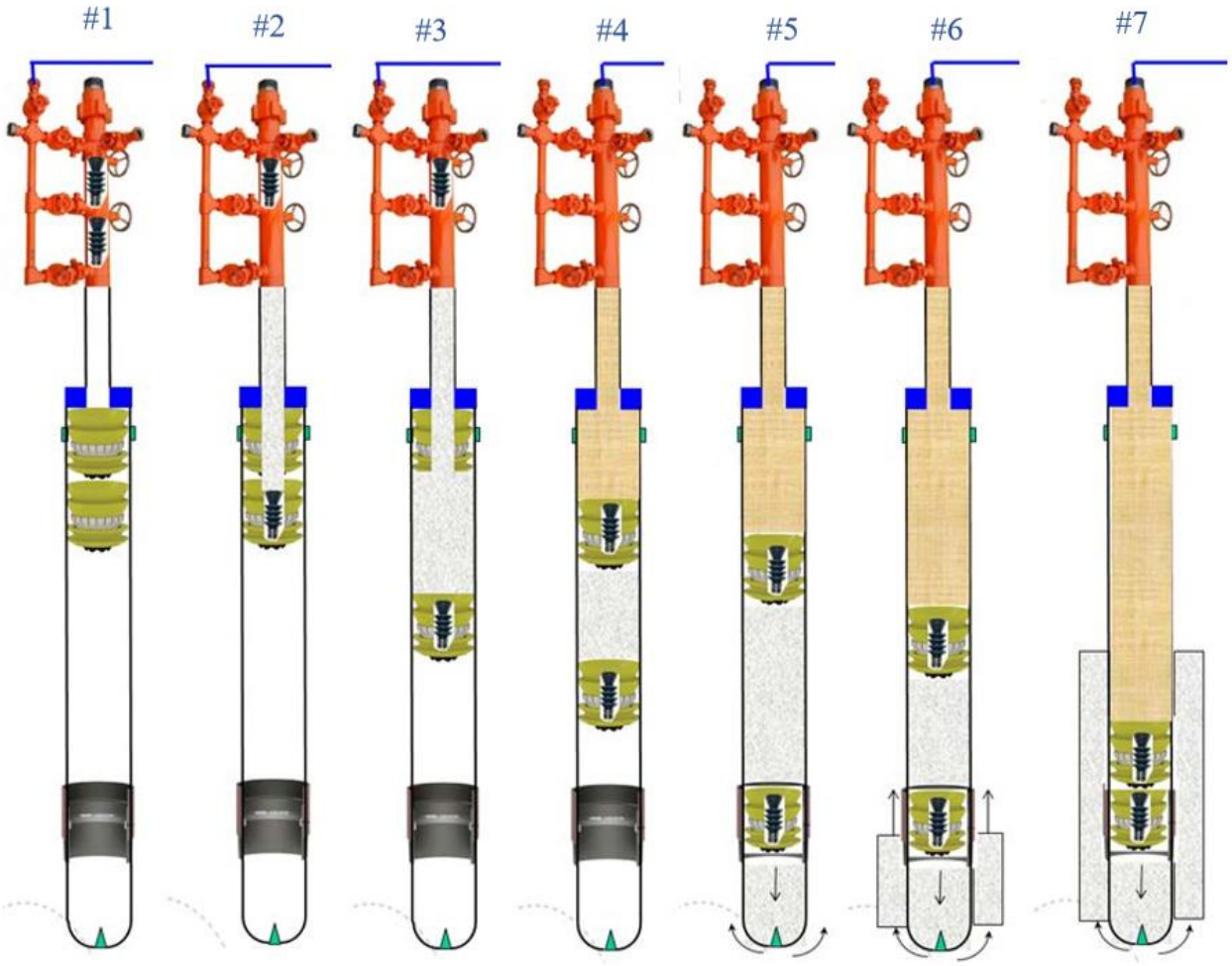

Figure 34: Steps in conventional cementing of casing strings (Brechan et al. 2017)

Appendix E: Illustration of the Physical Case

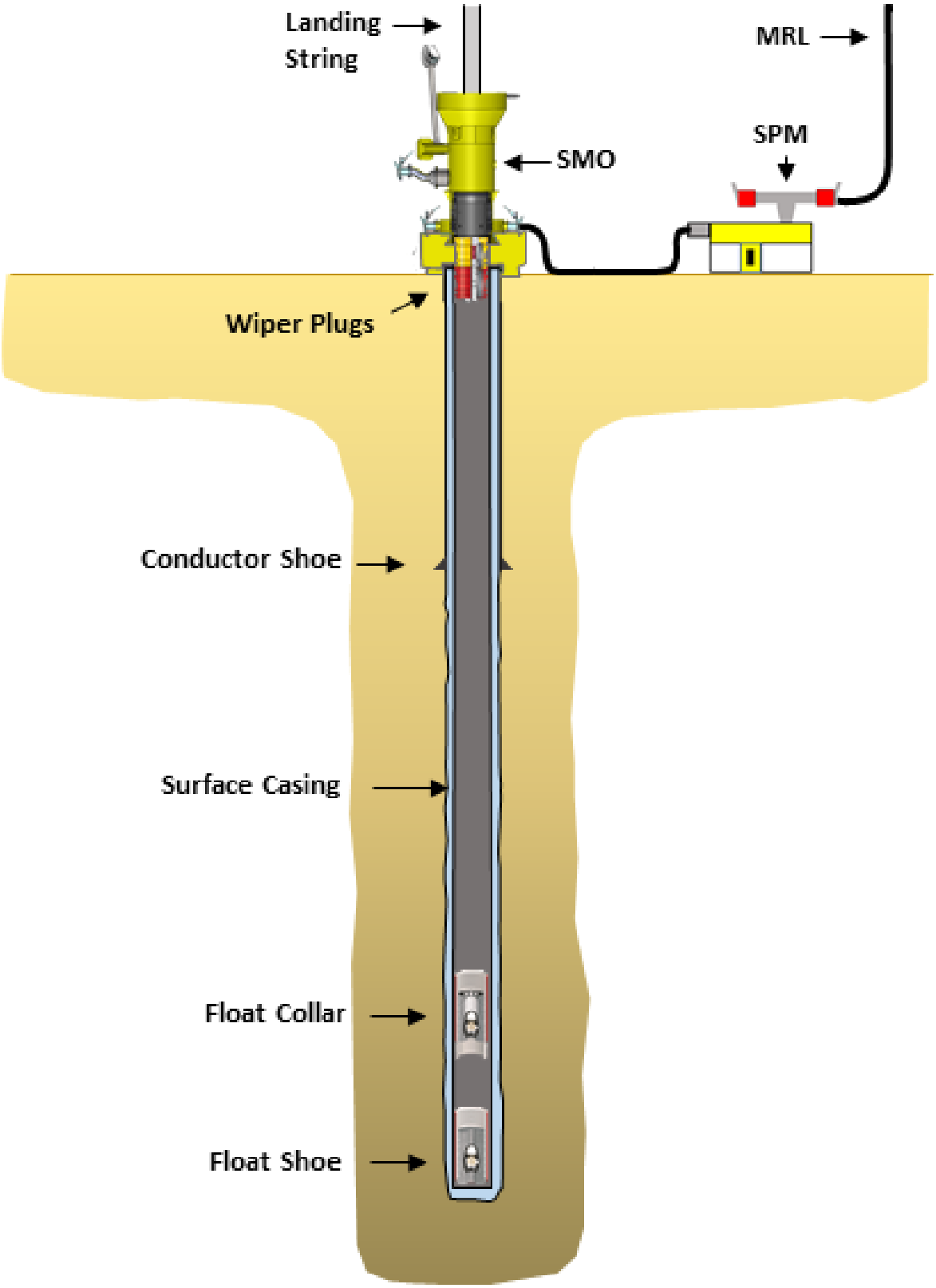

Figure 35: Sketch of the physical case that was modelled (made by the author, with cuts from (Weatherford International 2005), (Weatherford International 2013) and (Elahifar 2020)

Appendix F: Overview Digital Model

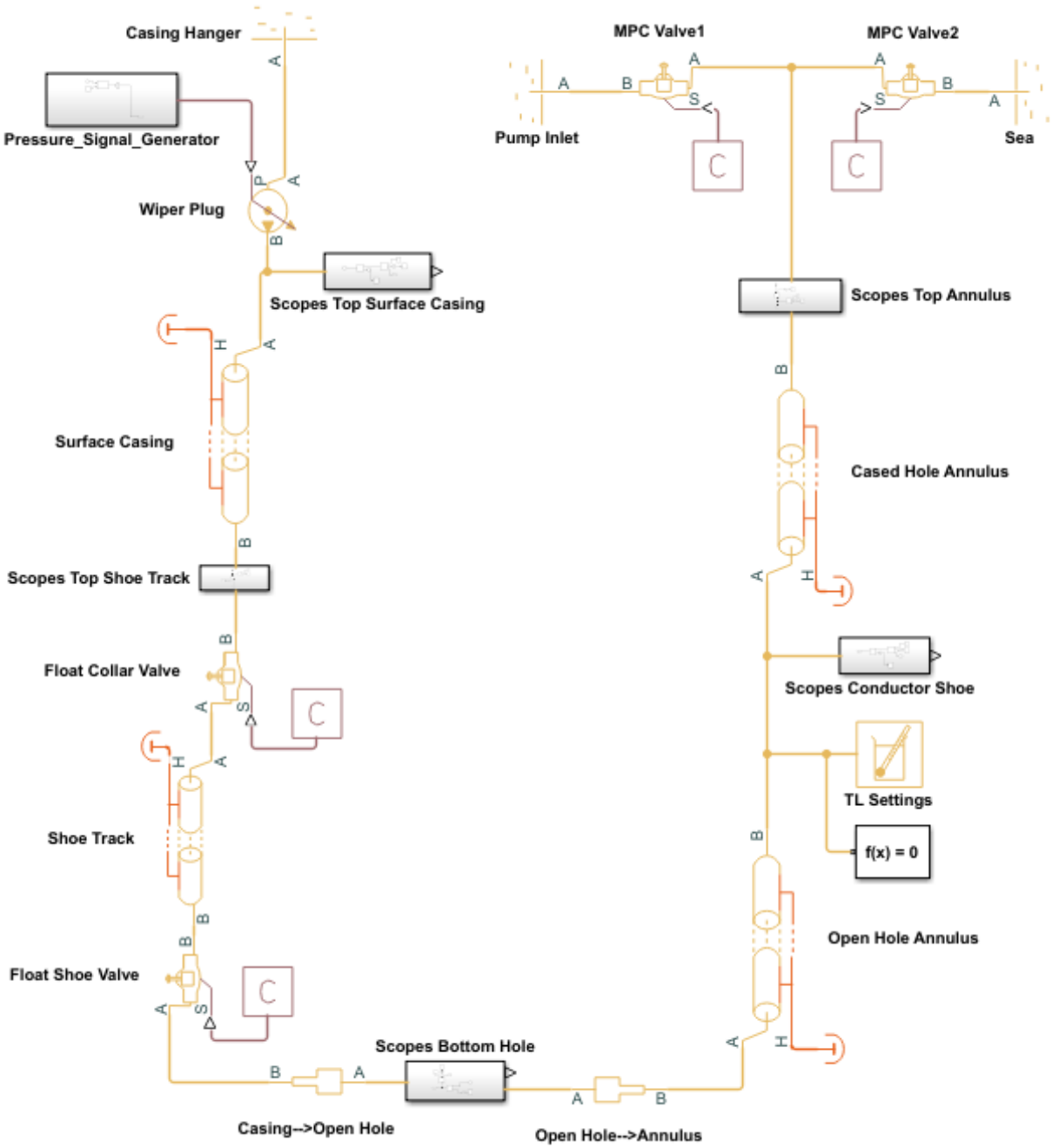

Figure 36: Illustration of the digital model in block scheme format (cut from model)

Appendix G: Block Descriptions

All blocks used for modelling the physical part of the system are presented below. The block names refer to the block library in the Simscape fluid software. The descriptions provide information on which system components the block represents. All figures in this appendix are copied from the Simscape Fluid reference guide, which is cited as: The MathWorks Inc. (2020a) in the reference list.

	Block name: Pipe (TL) **Description:** This block is used for modelling fluid filled conduits and it represent a major part of modelled system. In the model, this block is used for representing the surface casing, shoe track, open hole annulus and the cased hole annulus.
	Block name: Thermal Liquid Settings (TL) **Description:** This block defines the physical properties of the fluid in the system. In the model, this block receives the selected properties from the Matlab script and assign them to the fluid before simulation is initiated.
	Block name: Controlled Pressure Source (TL) **Description:** This block models an ideal pressure source that recreates a physical pressure signal based on the input signal through port P. In the model, this block represents the wiper plug and it generates the pressure transient from releasing the plug.
	Block name: Gate Valve (TL) **Description:** This block is used for modelling a flow restriction. In the model, this block represents the float collar and float shoe, but also the MPC- valves, situated on top of the annulus.
	Block name: Reservoir (TL) **Description:** This block defines the boundary conditions for the fluid system. In the model, this block represents the conditions inside the casing hanger at one end and the conditions at MPC-valves on the other end.
	Block name: Sudden Area Change (TL) **Description:** This block is used for modelling pressure loss across sudden changes of cross section area. In the model, this block is used at bottom hole to represent the transition from surface casing to open hole and the transition from open hole to annulus

NTNU

Norwegian University of
Science and Technology